Major, trace, and rare earth element geochemistry of the Oligocene Chiatura stratiform manganese oxide/hydroxide deposit, Georgia

Bilge SASMAZ[1], Ahmet SASMAZ[1], and James R. Hein[2]

[1]Firat University
[2]United States Geological Survey

November 23, 2022

Abstract

The Chiatura deposit is considered one of the world's largest deposits of metallurgical grade manganese, yet its geochemistry is poorly known, which is the focus of this paper. The Oligocene sedimentary manganese deposit is located in the Chiatura region of central Georgia and formed on stable crystalline basement in a restricted arm of the Paratethys during a transgressive-regressive cycle. The average main trace element contents of the samples are 3944 ppm Ba, 946 ppm Sr, 511 ppm Ni, 150 ppm Zn, 94 ppm V, 84 ppm Cu, and 55 ppm Co. The trace element concentrations of the manganese oxide ore are generally low and indicate an enrichment assemblage of V, Co, Ni, Cu, Zr, Ba, As, Cd, Pb, and Zn. The total rare earth element (REE) concentrations of the deposits vary from 83 ppm to 521ppm, with a mean of 199 ppm. All manganese-oxide samples have negative Ce anomalies (mean 0.58) and generally positive Eu anomalies. All geochemical data indicate that the Chiatura manganese-oxide ores formed rapidly within oxic seawater as reflected by the negative Ce anomalies. The mixed oxide and carbonate ores formed at deeper-water depths compared to the oxide-hydroxide ores in the Chiatura region. Also, our results point out that the metals were transported from both terrestrial sources (Pb isotopic data) and a hydrothermal source in deeper water (chemical discrimination diagrams). The metals associated with the Mn-oxide ores likely formed syngenetically through microbially mediated mineralization at water depths deeper than the area where the carbonate-ore deposits formed.

Major, trace, and rare earth element geochemistry of the Oligocene Chiatura stratiform manganese oxide/hydroxide deposit, Georgia

Ahmet Sasmaz[a*], Bilge Sasmaz[a], James R. Hein[b]

[a] Firat University, Department of Geological Engineering, 23119, Elazig, Turkey
[b]U.S. Geological Survey, 2885 Mission St., Santa Cruz, CA, 95060, USA

Abstract

The Chiatura deposit is considered one of the world's largest deposits of metallurgical grade manganese, yet its geochemistry is poorly known, which is the focus of this paper. The Oligocene sedimentary manganese deposit is located in the Chiatura region of central Georgia and formed on stable crystalline basement in a restricted arm of the Paratethys during a transgressive-regressive cycle. An Oligocene basal conglomerate is overlain by sandstone that is in turn overlain by the ore deposits. The Chiatura sedimentary deposits form horizontal beds, 1.5 to 4 m thick, average 2 m, of which 1 to 1.5 m is high-grade ore, covering an area of some 150 km^2. The Chiatura deposit contains three types of ore, primary oxide ores, carbonate ores, and oxidized carbonate ores and this paper focuses on the oxide ores. The common manganese minerals in the oxide ore are manganite, pyrolusite, braunite, and psilomelane, and less commonly bixbyite, rhodochrosite, and vernadite. Eighteen manganese oxide and four wall rock (low manganese content) samples were analyzed for major oxides and trace and rare earth elements. The key mean major oxide contents of the manganese ores are 36.6 wt.% MnO, 2.45 wt.% Fe_2O_3, 23.5 wt.% SiO_2, 5.88 wt.% Al_2O_3, and 3.84 wt.% CaO. The average main trace element contents of the samples are 3944 ppm Ba, 946 ppm Sr, 511 ppm Ni, 150 ppm Zn, 94 ppm V, 84 ppm Cu, and 55 ppm Co. The trace element concentrations of the manganese oxide ore are generally low and indicate an enrichment assemblage of V, Co, Ni, Cu, Zr, Ba, As, Cd, Pb, and Zn. The total rare earth element (REE) concentrations of the deposits vary from 83 ppm to 521ppm, with a mean of 199 ppm. The PAAS-normalized REE patterns have similar trends and show heavy REE (HREE) enrichments. All manganese-oxide samples have negative Ce anomalies (mean 0.58) and generally positive Eu anomalies (mean 1.20), except for four samples. All geochemical data indicate that the Chiatura manganese-oxide ores formed rapidly within oxic seawater as reflected by the negative Ce anomalies. The mixed oxide and carbonate ores formed at deeper-water depths compared to the oxide-hydroxide ores in the Chiatura region. Also, our results point out that the metals were transported from both terrestrial sources (Pb isotopic data) and a hydrothermal source in deeper water (chemical discrimination diagrams). The metals associated with the Mn-oxide ores likely formed syngenetically through microbially mediated mineralization at water depths deeper than the area where the carbonate-ore deposits formed.

Key words: Manganese-oxide ore, trace elements, rare earth elements, Chiatura, Georgia

1. INTRODUCTION

The Oligocene stratiform manganese deposit at Chiatura, Georgia, together with the similar Nikopol (Ukraine) deposits contains up to 80% of the world's onshore reserves of manganese (Maynard, 1983). The Chiatura manganese deposit in western Georgia is within the Dzarula Massif and has a total reserve of commercial and economic manganese ore estimated to be 240 million tons, defined as 41.6% oxide ore, 39% carbonate ore, and 19% hydroxide ore (Strishkov and Levine, 1987). The deposits were discovered in 1849 by the well-known Georgian poet Akaki Tsereteli and the first

mining activities in the region started in the 19th century along with archaeological excavations around Chiatura. Chiatura is defined as the city of “Manganese and Ropeways", and showed evidence of metallurgical processing and mining of manganese and iron ores in ancient times (Bronze or Iron age) (Khamkhadze, 1982; 1984).

Manganese deposits associated with sedimentary environments may contain concentrations of rare earth elements (REE) (Chakhmouradian and Wall, 2012). The REE may occur within the manganese minerals due to ion substitution (Dill et al., 2011) or through sorption on Mn oxides or associated Fe oxides. Manganese deposits and their REE geochemistry have been used to better understand the sedimentological and geochemical conditions during the formation of manganese minerals and their host deposits (McLennan, 1989; Dubinin 2006; Hein et al., 2013; Hein and Koschinsky, 2014; Sasmaz et al., 2014; Hein et al., 2017; Konstantinova et al., 2017; Chen et al., 2018; Vereshchagin et al., 2019) and to determine the genesis of hydrothermal systems and physicochemical parameters of depositional environments (Akgul, 2015; Roy et al., 2018; Tobia, 2018; Sasmaz et al., 2018; Sinanoglu and Sasmaz, 2019). Based on the chemical composition and geological settings of Fe-Mn deposits, they can be divided into three groups, namely diagenetic, hydrogenetic, and hydrothermal (Hein et al., 1997; Bau et al., 2014; Josso et al., 2017). Many papers have been published on the isotope geochemistry, mineralogy, and petrography of the manganese carbonate ores in both Chiatura and Nikopol manganese deposits (Bolton and Frakes, 1985; Hein and Bolton, 1994; Varentsov, 2002; Varentsov et al., 2003; Kuleshov and Bych, 2002; Kuleshov, 2003; Kuleshov and Brusnitsyn, 2005; Maynard, 2010) but not on the geochemistry of the manganese oxide/hydroxide deposits at Chiatura. Here, we investigate the conditions of formation of the Chiatura manganese oxide/hydroxide deposit, and the abundances of major oxide, trace elements, and REE at various stratigraphic levels within the manganese deposit.

2. GEOLOGICAL SETTING OF THE CHIATURA MANGANESE DEPOSIT

The geological history of the Chiatura and the mineralogical and petrographical properties of manganese deposits are largely summarized by Varetsov and Rakhmanov (1980) and Roy (1981). A belt of early Oligocene manganese deposits extends for two to three hundred kilometers through Georgia and Ukraine, and south along the west side of the Black Sea into Bulgaria (Fig. 1). This belt contains the largest manganese ore deposits in the former Soviet Union, the most important of which is the Chiatura deposit in Georgia. The transgressive sequence of Oligocene ores at Chiatura overlies Cretaceous limestone. The Oligocene section is composed of a basal conglomerate overlain by sandstone that is in turn overlain by the ore beds. The ore occurs as carbonates (about 40% of the reserves) and as primary and supergene oxides (Hein and Bolton, 1994).

Tectonically, the Chiatura deposit lies in the Georgian part of the Transcaucasus median massif. The Georgia part comprises Paleozoic and Precambrian crystalline rocks overlain by volcanogenic-sedimentary rocks and terrigenous carbonate of Cenozoic and Mesozoic ages. The Chiatura deposit is located near outcrops of these older crystalline rocks (including schists, gneisses, and granitoids), which are part of the Dzirula Massif. Generally, the ore-bearing Oligocene and Miocene sedimentary deposits unconformably overlie Late Cretaceous limestone which, in turn, lies directly on the crystalline basement. In places, however, and particularly in the western part of the deposit, ore-bearing sedimentary rocks rest directly on crystalline basement. The sequence is structurally undeformed except where disrupted by minor faults bordering the ore section on the north and northwest. These have undergone repeated vertical oscillations during the Mesozoic and Cenozoic. A summary of stratigraphic relationships in the Chiatura deposit is shown in Fig. 2 (Bolton and Frakes, 1985).

The Oligocene formation containing manganese deposits mainly consists of authigenic silicates, oxides, carbonate, phosphates, sulfides, and manganese sections (Fig. 2). This formation transgressively covers Late Cretaceous limestone in

the extreme western part of the basin. The Oligocene manganiferous deposit is between 30 and 150 m thick and is overlain by late Oligocene units and Miocene slate, claystone, limestone, and sandstone. The Late Cretaceous limestone and early Oligocene ore-bearing sedimentary rocks show horizontal layering or in places an eastward dip between 1° and 4°. The manganese deposit is covered by terrigeneous rocks consisting of greenstone, sandstone, and feldspar-quartz sands; manganese-bearing sandstone and phosphorite are scarce. The manganese-bearing layer has a thickness between 0.2 to 16 m and consists of a series of lenticular ore layers. As many as 18 ore beds up to 0.5 m thick occur, each interbedded with sandstone and shale, which are locally calcareous and siliceous. The mineralized sequences are as thick as 25 m. The interlayers vary from 2 to 26 m (commonly 5-8 m) and contain abundant silica minerals, smectites, and other authigenic components. The ore-bearing section in the southwestern part of the basin is cut by faults shown on Figure 2 (www.ifsdeurope.com).

The Chiatura ores have been divided into five petrographic types by Varentsov and Rakhmanov (1980), such as oxidic, carbonate, oxidized, metamorphosed, and supergene ores. Sedimentary oxidic and carbonate ores are the dominant ore types and account for 86% of the total reserves of the deposit. Oxidic ores in the upper zone of the manganese deposit are composed of psilomelane, pyrolusite, and manganite and display a dark color in the field (Figs. 3, 4); they occur mainly as nearly spherical, concentrically laminated particles (ooliths, pisoliths) up to ~20 mm in diameter and set in either a matrix of sandy claystone, manganese oxides, or manganese carbonates. Complex oolitic ores with manganite and rhodochrosite laminae occur at the base of the mineralization, showing more pale colors. Oxidized supergene ores represented by vernadite, rancieite, and pyrolusite-psilomelane are produced by alteration of sedimentary oxides and carbonates. Contact metamorphosed ores are localized near contacts with rare basaltic dikes that penetrate the deposit. They are composed mainly of braunite, ramsdellite, and hausmannite (Varentsov and Rakhmanov, 1980). Supergene ores are sandstones and argillaceous cherty rocks impregnated by manganese hydroxides, psilomelane, and pyrolusite mobilized and deposited during the weathering cycle (from Hein and Bolton, 1994). Strishkov and Levine (1987) mentioned that the manganese of Chiatura ores derived from weathering of nearby quartz porphyry veins and granitic rocks that were dissolved, transported, and precipitated as replacement of Oligocene sediments.

Ore bodies in the northern and southwestern parts of the study area are mostly of high manganese contents. The manganese contents and thickness of the deposits gradually increase toward the eastern part from the western basin. The carbonate and oxide ores in this region are lenticular and manganese ore grades decrease in the slope direction. The manganese-forming process in the study area generally began with the deposition of carbonate ores. The rhodochrosite and manganocalcite in the Perevisi and Rgani ore regions occur in trace amounts. The hydrogoethite and goethite intervals (1-2 m-thick) in the lower part of the ore body were seen at the boundary between the oxide and carbonate ores. Silicate minerals are abundant whereas sulfide minerals are restricted spatially to the carbonate ores. Carbonate fluorapatite occurs in the oolite centers, together with manganocalcite, rhodochrosite, opal, and ferrous montmorillonite.

3. SAMPLES AND ANALYTICAL METHODS

3.1. Sampling

Twenty-two primary manganese oxide-hydroxide samples and host rock (18 Mn oxide-hydroxide + 4 wall rocks with low Mn content) were collected from the oxide-hydroxide part of Chiatura Mn deposit for major oxides, trace elements, and rare earth element analyses. The different ore types were sampled from the bottom of the upper manganese ore section seen in Figures 3 and 4. Oxide-hydroxide ores (CHY-1, CHY-3) occur in the upper section, wall rocks with high Mn content (CHY-5, CHY-6), and wall rocks with low Mn content (CHY-2, CHY-4) in the lower part of the central

section (Fig. 4). These samples were analyzed to obtain trace element changes through this section. In Figure 4, the dark sections mostly contain manganese oxide-hydroxide ores and less limestone, quartz and clay minerals, the pale-colored sections contain mostly limestone, quartz and clay minerals, and less manganese ore.

3.2. Analytical Methods

The 22 samples were broken up and milled to a 200-mesh size for analyses of major oxides by ICP-AES, and trace and rare earth elements by ICP-MS. Repeated analyzes showed better than 5% reproducibility. All ICP-AES and ICP-MS analyses were performed by Acme Analytical Laboratories in Canada. Powdered manganese samples (50 mg) were digested in a mixture of $HCl:HNO_3:H_2O$ (1:1:1, v/v; 6 ml per 1.0 g of sample) for 1 hour before analyses.

Pb isotopes (^{208}Pb, ^{207}Pb, ^{206}Pb, and ^{204}Pb) were determined for all manganese oxide-hydroxide samples, by the ICP-MS method at Acme Laboratories (Canada). These samples were dissolved with aqua regia (3HCL + 1 HNO_3 mixture) and analysed for $^{206}Pb/^{204}Pb$, $^{207}Pb/^{204}$, and $^{208}Pb/^{204}Pb$ isotope ratios. The NIST-SRM 981 standard was used during the analyses with the following results: $^{206}Pb/^{204}Pb$ 16.9374; ^{207}Pb /^{204} Pb 15.4916; $^{208}Pb/^{204}Pb$ 36.7219. For these ratios, reproducibility and precision during an 8-hour period (error ±% RSD) were ± 0.27%, ± 0.20%, and ± 0.17%, respectively.

The data were statistically analyzed using the Student Newman Keul's Procedure (SNK) (Sokal and Rohlf, 1995) with SPSS 15.0 software and variance analysis (ANOVA).

The corresponding values to calculate Ce and Eu anomalies for each sample were normalized to PAAS by using the formulas (Taylor and McLennan, 1985): $Ce/Ce^* = Ce_n /\sqrt{[La_n * Pr_n]}$, $Eu/ Eu^* = Eu_n /\sqrt{[Sm_n * Gd_n]}$, $Y/Y^* = Y_n/\sqrt{[Dy_n * Ho_n]}$.

3.3. Quality Assurance

All facilities have ISO accreditations and registrations of the Quality Assurance have been performed by recognized organizations. These accreditations and registrations meet the requirements of the ISO standards. All BVM facilities are registered to ISO 9001. Also, they have received ISO/IEC 17025 accreditation for specific laboratory procedures.

4. RESULTS AND DISCUSSION

4.1. Major Oxide Geochemistry

The chemical composition of primary manganese oxide-hydroxide samples is given in Table 1. The MnO contents in the Chiatura manganese deposits vary from 3.87 to 58.4 wt.% with an average of 35.5%, except for a few silica-rich samples (CH-11, CHY-02 and CHY-04) collected from the manganese deposits. The major oxide contents of the Chiatura manganese deposit range from 4.88 to 77.0% SiO_2, 0.58 to 21.7% CaO, 1.73 to 14.8% Al_2O_3, and 0.89 to 5.91% Fe_2O_3 (Table 1). Bivariate plots for n=22 of SiO_2 versus K_2O (r= 0.93), SiO_2 versus Al_2O_3 (r= 0.65), and SiO_2 versus TiO_2 (r= 0.58) show positive correlations whereas SiO_2 versus MnO (r= -0.84) and SiO_2 versus Sr (r= -0.65) show strong negative correlations. Positive correlations of SiO_2 with K_2O, Al_2O_3, and TiO_2 reflect terrigenous detritus input to the depositional basin. Compared to the Binkılıc manganese deposit (Gultekin and Balci, 2018), the Chiatura manganese deposit has higher SiO_2 and Al_2O_3 contents and a lower mean CaO content.

The Chiatura manganese-oxide deposit chemical data were plotted as Si versus Al and Na versus Mg, discrimination diagrams to determine the genetic origin and depositional environment (Fig. 5; Choi and Hariya, 1992;

Nicholson, 1992). These diagrams indicate that the Chiatura manganese-oxide deposit formed as hydrogenetic precipitates, possibly in fresh-water or shallow-marine environments. However, data plotted on trace element discrimination diagrams tell a different story (next two sections).

4.2. Trace Element Geochemistry

The total trace element concentration in the manganese samples ranged between 1511 and 11254 ppm (Table 2), compared to mean marine sediments, 760 ppm (Turekian and Wedepohl, 1961). Mean concentrations for some of the higher-content trace elements are V (94 ppm), Co (57 ppm), Ni (530 ppm), Cu (86 ppm), Sr (984 ppm), Y (54.8 ppm), Ba (4096 ppm), As (25 ppm), and Zn (154 ppm). The Chiatura manganese samples contain more Co, Ni, Cu, Sr, Y, Ba, As, Cd, U, and Zn and lower V, Cr, Rb, Zr, Nb, Hf, Th, and Pb compared to Post Archean Australian Shale (PAAS) (Taylor and McLennan, 1985) (Fig. 6). While the Sr and Ba from the large-ion lithophile elements are highly enriched, Rb is depleted compared to PAAS (Fig 6). The PAAS-normalized ferromanganese-hosted trace elements (Co, Ni, Cr, and V) showed strong enrichments together with As, Cd, and Cu, except for V and Cr (Fig. 6). Among the high field strength element (HFSE; Y, Zr, Hf, Nb, U and Th), Nb, Zr, Hf, and Th are signicantly less compared to PAAS. The average Mn/Fe, Co/Zn, Co/Ni, and Zr/Hf ratios in the Chiatura manganese deposits are 24, 0.37, 0.11, and 57, respectively (Table 2).

Discrimination diagrams for trace element concentrations in the Chiatura manganese-oxide ores, Mn–Fe–(Ni + Co + Cu)x10 (Bonatti et al., 1972; Crerar et al., 1982), Zn–Ni–Co (Choi and Hariya, 1992), and Co/Zn–Co + Ni + Cu (Toth, 1980), indicate a primarily diagenetic or hydrothermal origin for the Bonatti diagram and hydrothermal origin for the other two diagrams (Fig. 7). This contrasts with the Choi and Hariya (1992) diagram (Fig. 5) that indicates a predominantly hydrogenetic origin.

Table 3 shows the major oxide and trace element contents of different manganese deposits distributed worldwide. The major oxide and trace element contents of the Chiatura manganese deposit are similar with those of the Binkilic, Cayirli, Kasimaga, and Elazig Mn deposits in Turkey (Gultekin, 1998; Gultekin and Balci, 2018; Oygur, 1990; Koc et al., 2000; Sasmaz et al., 2014) (Table 3). The relationships between Mn and Fe for various deposits are Mn:Fe <1 for lacustrine deposits, Mn:Fe = ~1 for modern hydrogenetic deposits (varies from ~0.5-2 for modern marine deposits), Mn:Fe = 0.1-10 for SEDEX deposits, Mn:Fe = 0.63 for SEDEX manganese deposits around Elazig, Turkey, modern hydrothermal Mn deposits = 15-40 (Hein et al., 1997) and Mn:Fe = mean 16.76 (5.38 to 58.31) for the Binkilic sedimentary manganese deposit, Turkey (Gultekin and Balci, 2018). The Mn:Fe ratios of Chiatura manganese deposit range between 0.9 and 62.9 (average = 23.7) (Table 3) and have similar values with Binkilic sedimentary manganese deposits (Gultekin and Balci, 2018). Whereas higher Mn/Fe ratios may indicate higher O_2 levels, lower Mn/Fe ratios indicate lower dissolved O_2 concentrations in the water column. Under anoxic conditions Mn shows more rapid reduction than Fe (Loizeau et al., 2001) and Fe accumulation occurs. High Mn/Fe ratios occur predominantly under oxidic conditions and high amounts of Mn accumulation takes place (Naeher et al., 2013).

The Zr/Hf ratios vary from 25 to 83 with an average of 57 and the Nb/Ta ratios vary between 0.5 and 7.5 with an average of 3 (Table 2). The Nb/Ta ratios are lower compared to Pacific Ocean, Atlantic Ocean, and Southern Ocean water, North Atlantic, Pacific, and Southern Ocean Deep Waters, and Atlantic and Pacific Fe-Mn crusts (Godfrey et al., 1996, 2009; Firdaus et al., 2011; Schmidt et al., 2014; Censi et al., 2010, 2017, 2018, 2019) but the Zr/Hf ratios are comparable to Pacific and Atlantic Fe-Mn crusts and North Atlantic Deep Water (Fig. 8). The HFSE enrichments in hydrogenetic oxides result from absorption from seawater (Firdaus et al., 2011; Schmidt et al., 2014). This also shows

that the low Zr/Hf and Nb/Ta ratios in the studied manganese oxide ores indicate a low HFSE content in the seawater during the formation of the Chiatura manganese deposit or a different sorption capacity of the Chiatura Mn minerals compared to the vernadite and iron oxyhydroxides in modern Fe-Mn crusts.

4.3. Rare Earth Element Geochemistry

The ΣREE concentrations of the Chiatura manganese samples vary between 83 ppm and 521 ppm with an average of 199 ppm (Table 4). The ΣREE contents of manganese oxides with high Si are very low; samples (CH-07, CH-10, CH-16) containing Mn contents between 40 and 50% have the highest ΣREE concentrations. The PAAS-normalized REE patterns (Taylor and McLennan, 1985) of the manganese samples exhibit similar trends and show a heavy REE (HREE) enrichment (Fig. 9). The average REE sequence in the PAAS-normalized REE pattern is as follows: MREE (9.91) > HREE (8.32) > LREE (4.32) (Fig. 9). The La_n/Yb_n ratios are used to determine the fractionation of the light and heavy REE contents and the ratios for the Chiatura manganese samples range from 0.22 to 1.87 with a mean of 0.92, verifying the HREE enrichment.

Cerium is probably the most efficaceous element of the REE series to use as a discriminating element for deep-water Fe-Mn deposits because it readily oxidizes and is continuously and irreversibly removed from seawater at the surface of Mn oxides (Takahashi et al., 2007); therefore, positive Ce anomalies in Fe-Mn oxide deposits are considered typical of hydrogenetic deposition. Due to differences in the kinetics among different Fe-Mn deposits and irreversible Ce uptake from seawater, Ce will be most enriched in hydrogenetic deposits, lower in diagenetic deposits, and lower yet in hydrothermal deposits (Josso et al., 2017). The Ce/Ce* and Eu/Eu* ratios have been used as an indicator of redox state and to estimate the physicochemical characteristics of hydrothermal fluids or the depositional environment including redox conditions, pH, and temperature (Bau and Möller, 1992; Bau, 1996).

All the manganese-oxide samples studied have negative Ce anomalies (0.24 to 0.91, mean 0.58), indicative of rapid deposition of the manganese oxides, which does not leave time for the surface oxidation of the Ce and thus the Ce/Ce* reflects that of seawater (e.g. Bau et al., 2014; Tostevin et al., 2016). Carbonates typically have low REE contents and a negative Ce anomaly also matching that of seawater. However, carbonates can have a positive Ce anomaly, which typically reflects inheritance from mineralization via the reduction of a Mn oxide-hydroxide (e.g. Polgári et al., 2012). These data indicate that seawater may have been the mineralizing fluid for both the oxide and carbonate ores via chemical or colloidal precipitation-accretion, biogenic carbonate or silica deposition and subsequent mineralization, low-temperature hydrothermal precipitation, or shallow-water diagenetic processes such as characteristic of manganese deposits in the Baltic Sea (Table 1) (Hein and Bolton, 1994; Emelyanov, 2011). Under seawater Eh and pH conditions, dissolved Ce is primarily Ce^{3+} forming predominately carbonate complexes. It oxidizes to Ce^{4+} via surface reactions on the manganese oxides, although in surface waters Ce^{3+} can oxidize to Ce^{4+} through bacteria-mediated reactions forming CeO_4, which is strongly particle reactive. Once Ce is oxidized on the surface of Mn oxides, it is no longer desorbed, leaving seawater depleted in Ce relative to the trivalent REEs. This Ce fractionation only occurs under oxic conditions (German and Elderfield, 1990; German et al., 1991).

Most of the manganese-oxide samples have positive Eu anomalies (except CH-08, CH-09, CHY-01, CHY-03) with a range of 0.58 to 1.54 (mean 1.20) (Table 3). The positive Eu anomaly may indicate that hydrothermal fluids were involved in the mineralization (Abiding and Calagari 2015; Tobia 2018). The positive Eu anomalies would indicate the existence of Eu^{2+} during deposition from the suboxic hydrothermal fluids. However, feldspar enrichment in diagenetic environments may also lead to a positive Eu anomaly (Roy et al., 2018). A positive Eu anomaly can also be produced by

co-precipitation together with Eu-enriched minerals. The three samples with negative Eu anomalies can be explained by the lack of leaching of plagioclase by the hydrothermal fluids or by precipitation of Eu-rich minerals, such as barite or anhydrite, at depth of the hydrothermal system (Hein et al., 1997, 2017).

REE alone or combined with other elements can indicate the origins of the Fe-Mn-oxide deposits (Bau et al., 2014, Josso et al., 2017). Commonly used ternary diagrams may not clearly differentiate Fe-Mn deposits formed by mixed genetic processes (Josso et al., 2017). The Ce (Ce, Ce/Ce*), Y, Ho, Nd, and Zr concentrations can be used as a guide for investigating the genesis of manganese-oxide samples (Bau et al., 2014; Josso et al., 2017). Our samples were plotted on the genetic discrimination diagrams along with several typical examples of diagenetic, hydrogenetic, and hydrothermal Fe-Mn deposits for comparison (Zeng et al., 2012; Bau et al., 2014; Josso et al., 2017). Both $(Ce/Ce^*)_n$ vs Nd and Ce vs (Co+Ni+Cu)/1000 diagrams (Fig. 10a,b) show that the Chiatura samples plot with diagenetic samples. Although diagenetic deep-ocean Fe-Mn nodules usually show a negative Ce anomaly (Fig. 10a,b), the Nd concentrations in diagenetic manganese have higher concentrations than those of hydrothermal manganese and vary between 10 and 100 ppm (Bau et al., 2014; Vereshchagin et al., 2019). On the Ce vs Zr diagram (Fig. 10c), the Chiatura samples data span the area between the diagenetic and hydrothermal fields proposed by Bau et al. (2014) (Fig 9c). The $(Ce/Ce^*)_n$ vs $(Y/Ho)_n$ diagram shows that the Chiatura samples mostly plot within the area of hydrothermal manganese deposits (Fig. 10d). The $(Y/Ho)_n$ ratio indicates a decoupling of the geochemical twins Y and Ho, which produces Y anomalies within REY patterns due to the very similar ionic radius to Ho^{3+}, which suggests that Y^{3+} can be inserted into REE patterns between isovalent Dy^{3+} and Ho^{3+} (Bau, 1996). This decoupling results from preferential scavenging of Ho relative to Y on metal-oxide surfaces due to the lower stabilities of Y surface complexes (Bau, 1996;1999). These discrimination diagrams indicate that the Chiatura manganese oxide-hydroxide ores plot in similar areas with the Baltic Sea and Kara Sea shallow-water diagenetic nodules/concretions on the Ce/Ce* ratio *vs* Nd diagram and Ce vs Co+Ni+Co)/1000 diagram (Fig. 10a,b), with the deep-water Pacmanus hydrothermal samples and shallow-water, diagenetic Fe-Mn nodules from the Kara Sea on the Ce vs Zr diagram, and in the hydrothermal manganese area defined by Bau et al. (2014) in Ce/Ce* vs $(Y/Ho)_n$ diagram (Fig. 10c,d).

The Y concentrations in the Chiatura Mn-oxide samples vary from 19 to 137 ppm, with an average of 53 ppm (Table 4) and show positive Y anomalies that range from 0.67 to 1.54 with a mean of 1.09 (Table 4). In upper continental crust-normalized REY patterns (Cao et al., 2020), negative Ce and positive Y anomalies of the manganese oxides from the study area have patterns similar to those of deep-ocean Mn nodules (Flanagan and Gottfried. 1980) and modern mean seawater (Alibo and Nozaki, 1999; Zhang and Nozaki, 1996).

The Cape Vani (Milos Island, Greece) Mn-oxide and barite deposit shows the three-dimensional characteristics of a shallow-water hydrothermal system between Mn-oxide ores and barite deposits (Hein et al., 1999, 2000). The hydrothermal fluid was predominantly enriched seawater in metals leached from the basement rocks. The hydrothermal solutions were supported by convection driven by heating from a magma source. Mn-oxide mineralization and barite precipitation were syngenetic. We envision that fluids from a similar hydrothermal system contributed to the formation of Chiatura Mn-oxide deposits that combined with the production of Mn-oxides from diagenetic processes, thereby creating a mixed origin ore deposit. It is observed that similar barite and pyrite formations occur with the continuation of Koçkale manganese-oxide ore section in Maden Complex (Sasmaz et al., 2014).

4.4. Pb Isotope Geochemistry

The average Pb isotope ratios of Chiatura manganese samples are 39.5 for $^{208}Pb/^{204}Pb$. 15.9 for $^{207}Pb/^{204}Pb$ and 19.1 for $^{206}Pb/^{204}Pb$ (Table 2). The $^{207}Pb/^{204}Pb$ ratios are between 14.2 and 16.9, indicating that the Pb in the Chiatura manganese ores was mostly sourced from metals or fluids with an upper crust signature (Zartman and Doe, 1981; Wang et al., 2014). The Pb isotope ratios that may support a seawater Pb isotope source, as recorded by Fe-Mn crusts and pelagic sediments for example, are shown in $^{208}Pb/^{204}Pb$, $^{207}Pb/^{204}Pb$, and $^{206}Pb/^{204}Pb$ space (Fig. 11a,b). The ultimate source of the Pb dissolved in seawater was river input to the oceans, dissolution of wind-blown debris, and Pb derived from mid-ocean ridge basalts (MORB), island arcs, and young continental margins (von Blanckenburg et al., 1996). The Pb isotope distributions in deep water have been recovered from ferromanganese crust surfaces (von Blanckenburg et al., 1996) and indicate that the highest radiogenic compositions of the $^{206}Pb/^{204}Pb$ ratio are detected in the NW Atlantic (>19.1) whereas less $^{206}Pb/^{204}Pb$ values are observe in the central North Pacific (<18.7) and the Southern Ocean (<18.9). The highest values in the North Atlantic reflect weathering of the ancient cratonic areas of Greenland and northern Canada (von Blanckenburg and Nagler, 2001). The Pb isotope values of the shallowest-water within the present-day Mediterranean Outflow Water does not indicate important temporal changes, showing that it had the same Pb sources for the past 15 Ma. Pb isotope time series recording the evolution of NE Atlantic water masses over the past 15 Ma were measured on three ferromanganese crusts. The Fe-Mn crusts were recovered between ~700 and 4600 m water depths including within the present-day Mediterranean Outflow Water and the NE Atlantic Deep Water (Muiños et al., 2008). Andrieu et al. (1998) investigated the Pb isotopes of basalts and sulfides (Fig. 11c.d) from the Trans-Atlantic Geotraverse (TAG) along the slow-spreading Mid-Atlantic Ridge in the North Atlantic Ocean. The Pb isotopic composition of the TAG sulfides in the upper part of the oceanic crust indicates large-scale hydrothermal fluid circulation. The Pb isotopic compositions of both sulfides and hydrothermal vent solutions did not change in hydrothermal vents at the TAG sites (Andrieu et al., 1998).

In Fig. 11c,d, our Pb isotope data plot in the same space with terrigenous sediment and pelagic and biogenic sediments that reflect seawater ratios, and Mn nodules that reflect pore water ratios (e.g., von Blanckenburg et al., 1996). The Pb isotopic ratios indicate that the potential sources of the Pb in the Chiatura oxide-hyroxide manganese ores is seawater from a shallow-water marginal basin of the Tethys Ocean. This shallow-water marginal sea conclusion is consistent with the geological and geochemical evidence (e.g. Bolton and Frakes, 1985). The Pb isotope ratios are also consistent with a hydrothermal contribution to the ore deposits.

5. GENETIC MODEL OF THE CHIATURA MANGANESE ORES

The Oligocene sedimentary manganese deposit is located in the Chiatura region of central Georgia and was deposited on stable crystalline basement in a restricted arm of the Paratethys sea during a transgressive-regressive cycle. The transgressive sequence of the Oligocene ores overlies Cretaceous limestone and is composed of a basal conglomerate overlain by sandstone that is overlain by the ore deposits. The Chiatura deposit formed near shore along a wide embayment marginal to a shallow-water marine basin (Varentsov and Rakhmanov, 1980; Roy, 1981). However, there is much disagreement on the source of the metals and the precise mechanisms of manganese precipitation and concentration (Khamkhadze, 1980; Varentsov and Rakhmanov, 1980). Frakes and Bolton (1984) independently presented models for manganese sedimentation in an intracratonic settings with a focus on the apparent relationship between the precipitation and concentration of manganese, sea-level change, and anoxia. Both models envisage a slow enhancement of dissolve Mn in an oxygen-deficient basin during significant marine transgression. The precipitation and accumulation of Mn at concentrations well above those in normal marine waters are thought to occur in nearshore zones during the late stages of

transgression and early regression, coincident with a reoxygenation of the water column (Hein and Bolton, 1994). However, the upper parts of the section, show evidence of shallow-marine deposition, such as scarce fossils, traces of glauconite, and abundant plant remains, which indicates regression. Although the ores are generally said to have been deposited "during the transgression," their position relative to the beginning of the regression is uncertain. The early Oligocene was a time of profound climate change from a cool to a more arid climate with vigorous oceanic circulation and upwelling in the Oligocene and this climate transition period ended by middle Oligocene time. Increased eutrophication took place that manifested in increased fertility and productivity. These climatic and oceanic changes coupled with marine transgression promoted Mn-ore formation through decreasing supplies of clastic debris to the depositional basin, increasing development of a low-oxygen zone in the water column that stored Mn in solution, and increased cycling of that stored Mn to the sites of deposition (Hein and Bolton, 1994). In Fig. 12A, we provide a speculative model for manganese sedimentation at Chiatura based largely on the regional stratigraphic considerations of Bolton and Frakes (1985). Initial transgression in the Chiatura region during early to mid-transgression during the early Oligocene was marked particularly in the western and southwestern areas by deposition of a basal conglomerate. Deepening of the basin is indicated by upward fining to predominantly quartz-feldspar sands and sandy clays. As inundation of the land continued, addition of terrestrial organic matter, together with increased biologic productivity in certain parts of the deepening basin, led to oxygen depletion and eventually anoxia (Frakes and Bolton, 1984). There was increasing accumulation of fine-grained, organic-rich sediment beneath the anoxic parts of the basin while dissolved Mn, derived from weathering of bedrock surrounding the basin, was slowly concentrated to levels well above those in typical marine waters. Oxygenation of Mn-rich waters in shallow, marginal settings may have led to the initial precipitation of manganese as oxides and hydroxides and, possibly, in more reduced parts of the basin as carbonates. Any subsequent inundation of such Mn accumulations by oxygen-depleted water due to landward movement of the redox interface in association with transgression would have led to dissolution of the previously formed manganese-oxide phases. At peak transgression during the middle Oligocene, organic-facies sedimentation was at a maximum, and the dark, fine-grained Maikop clays were deposited in relatively deep water, offshore areas northeast of the Chiatura deposit. In nearshore regions, however, occurred deposition of a compressed sequence with nodular phosphorite and glauconite. This association of phosphatic and glauconitic phases with organic-rich facies, little or no terrigenous sedimentation, and sea-level high stand is frequently also observed to have occurred elsewhere (Riggs, 1984; Bolton and Frakes, 1985). In the initial stages of regression during the middle Oligocene, the supply of organic matter to the sediments from terrigenous sources and marine plankton decreased, leading to relative deepening of the redox interface and consequent widening of the oxygenated rim around the basin margin. This resulted in formation of abundant Mn micro-particulate material transported shoreward via tidal-lag effects (Sundby et al., 1981; Frakes and Bolton, 1984), and finally accumulated as the first significant manganese layers. Both the rate of precipitation and the preservation potential increased with increasing oxygenation of the water column in the margin area. Shallowing of the basin was accompanied by increasing energy levels, which led to inversely graded deposits of oolites and pisolites (Bolton and Frakes, 1985). During basin shallowing in the late regression during the late Oligocene and early Miocene, there was continued, although reduced, precipitation of Mn in oxygenated nearshore areas with rapid depletion of manganese in the basin reservoir. Sedimentation during late stages of regression was dominated by the deposition of quartz sands and spongiolite.

All geochemical data in this study indicate that the Chiatura manganese oxide ores formed rapidly within highly oxic seawater, reflected the negative Ce/Ce* anomalies seawater. The mixed oxide and carbonate ores formed at deeper water depths compared to the oxide-hydroxide ores in the Chiatura region (Fig. 11B). Also, our results point out that the

metals were transported from both terrestrial sources (Pb isotopic data) and a hydrothermal source at deeper water based on several chemical discrimination diagrams. The metals associated with the Mn-oxide ores likely formed syngenetically through microbially mediated mineralization at water depths deeper than the area where the carbonate-ore deposits formed (Fig. 12B). While the dissolved Mn was in the reduced state in anoxic parts in deeper basin, Mn in the upper part precipitated as $MnCO_3$ in a suboxic zone, and MnO_2 in an oxic zone. Due to transgression and regression in the region, in places there occurred both oxide-hydroxide manganese minerals together with Mn-carbonate ores in the suboxic zone (Fig 12B). Dekov et al. (2020) suggested that both terrestrial and marine-sourced volcanic ash falls caused significant increases in seawater dissolved manganese concentrations during the formation of manganese ores, which also may have contributed to the dissolved Mn in the Chiatura basin.

6. CONCLUSIONS

Compared to other terrestrial manganese deposits, the Chiatura manganese deposit has lower SiO_2 but the highest MnO contents, with the exception of the Koryu and Hinode deposits located in the Tokoro Belt of Japan (Table 3). The Fe_2O_3 contents are among the lowest compared other manganese deposits (Table 3), except for the Tokoro deposit of Japan, Hazara deposit of Pakistan, and the Kasimaga and Elazig deposits of Turkey (Table 3). Trace element contents of the Chiatura deposit show higher concentrations than in most of these other manganese deposits, except for the Hazara and Koryu deposits, especially in terms of Ba, Sr, Ni, and Co contents. The Chiatura manganese deposit has almost the same trace element content as the Binkiliç sedimentary manganese deposit in western Turkey, which formed in a similar sedimentary basin, around the Black Sea Region. Our major, trace element, and rare earth element geochemical data indicate that the Chiatura Mn-oxide ore formed in a near-shore zone during the late stages of transgression and early regression, coincident with oxygenation of the water column. The upper parts of manganese ores show evidence of shallow-marine deposition, such as scarce fossils, traces of glauconite, and abundant plant remains. A shallow-water continental-margin environment within the Tethys Ocean is supported by our geological and geochemical data. The composition of the Chiatura manganese deposit was influenced by both diagenetic and hydrothermal processes based on major oxide and trace element data as determined by discrimination diagrams (Figs. 5 and 7). The rare earth element and Pb isotope data indicate that the Chiatura manganese deposit formed in an environment charactrerized by an increase in oxygenation and pH or a decrease in temperature compared to ambient seawater. Reducing low-temperature hydrothermal fluids mixed with seawater, volcanogenic or hydrothermal input such as ash, and low Sr, Nb, and Hf and high Co, Cu, Ba, As, and Cd contents charactized the depositional basin. In the depositional environment, the conditions prior to the formation of the Chiatura deposits was dominantly low-temperature, low-redox, and low-pH conditions and after that, together with transgression and regression of the sea, the physicochemical conditions during the deposition of the Mn-oxide ore changed to higher redox and pH conditions and an increase in temperature based on Ce and Eu anomalies. The Chiature manganese deposit formed MnO_2 in oxic zone and $MnCO_3$ in suboxic zone by transport of dissolved Mn^{+2} from the anoxic zone.

Hein and Bolton (1994) indicated that the possible sources of carbon for the Mn carbonates in Chiatura were from seawater bicarbonate, dissolution of biogenic carbonate (originally a seawater source), and oxidation of organic matter. Carbon from the latter source would be isotopically light, whereas the other two sources were near 0‰ (±2‰). The carbon derived approximately equally from degradation of organic matter and seawater bicarbonate. Carbon for calcite was derived predominantly from seawater. These isotopic relationships coupled with correlations among S, Mn, and organic carbon contents favor formation of the Mn carbonates during early diagenesis from the coupled reaction of

organic matter oxidation and manganese reduction. Mn oxyhydroxide probably formed the initial precipitate and oxygen deficient seawater acted as a carrier and reservoir for Mn^{2+}. An initial oxyhydroxide precipitate is indicated by inherited small positive Ce anomalies on REE plots of the Mn carbonates. The Mn oxyhydroxides were converted to Mn carbonates during very early diagenesis. Hein and Bolton concluded that deposition was in shallow water, probably in local coastal embayments. The oxygen isotopes indicate a relatively low temperature of formation. The early Oligocene was a time of profound climate change when there was a transition from the warm equitable climate and sluggish oceanic circulation during the Cretaceous and middle Eocene, to a cool and more arid climate with vigorous oceanic circulation and upwelling in the Oligocene. Increased eutrophication took place that manifested in increased fertility and productivity. The climate transition period ended by middle Oligocene time. These climatic and oceanic changes coupled with marine transgression promoted Mn-ore formation through decreasing supplies of clastic debris to the depositional basin, increasing development of a low-oxygen zone in the water column that stored Mn in solution, and increased cycling of that stored Mn to the sites of deposition.

Acknowledgements

This work was financially supported by the Firat University-FUBAP Unit (MF.18.49) for financial supports.

References

Akgul B., 2015. Geochemical associations between fluorite mineralization and A-type shoshonitic magmatism in the Keban–Elazig area. East Anatolia. Turkey. J Afr Earth Sci, 111, 222–230.

Andrieu, A.S., Honnorez, J., Lancelot, J., 1998. Lead isotope compositions of the TAG mineralization, Mid-Atlantic Ridge, 26°08′N. In: Herzig, P.M., Humphris, S.E., Miller, D.J., Zierenberg, R.A. (Eds.). *Proceedings of the Ocean Drilling Program. Scientific Results,*Vol. 158.

Baturin, G.N., 2009. Geochemistry of ferromanganese nodules in the Gulf of Finland, Baltic Sea. Lith. Miner. Resour., 44 (5), 411–426.

Baturin, G.N. Dubinchuk. V.T. 2009. Composition of ferromanganese nodules from Riga Bay (Baltic Sea). Oceanology 49 (1). 111–120.

Baturin, G.N. 2011. Variations in the composition of ferromanganese concretions of the Kara Sea. Okeanologiya 51 (1). 153–161 (in Russian).

Bau M. 1996. Controls on the fractionation of isovalent trace elements in magmatic and aqueous systems: evidence from Y/Ho. Zr/Hf. and lanthanide tetrad effect. Contrib. Mineral. Petrol. 123. 323–333

Bau. M.. Möller. P.. 1992. Rare-earth element fractionation in metamorphogenic hydrothermal calcite. magnesite and siderite. Minerol. Petrol. 45. 231–246

Bau. M.. Dulski. P.. 1996. Distribution of yttrium and rare-earth elements in the Penge and Kuruman iron-formations. Transvaal Supergroup. South Africa. Precambrian Res. 79. 37–55.

Bau, M..Möller. P.. Dulski. P.. 1997. Yttrium and lanthanides in eastern Mediterranean seawater and their fractionation during redox-cycling. Mar. Chem. 56. 123–131.

Bau. M. 1999. Scavenging of dissolved yttrium and rare earths by precipitating iron oxyhydroxide: experimental evidence for Ce oxidation. Y-Ho fractionation. and lanthanide tetrad effect. Geochim. Cosmochim. Acta 63. 67–77.

Bau, M.. Schmidt. K.. Koschinsky. A.. Hein. J.R.. Kuhn. T.. Usui. A.. 2014. Discriminating between different genetic types of marine ferro-manganese crusts and nodules based on rare earth elements and yttrium. Chem. Geol. 381. 1–9.

Ben Othman, D., White, W.M., Patchett, J. 1989. The geochemistry of marine sediments. island arc magma genesis and crust-mantle recycling.
Earth Planet. Sci. Lett., 94, 1-21.

Bolton, B.R., Frakes, L.A. 1985. Geology and genesis of manganese oolite. Chiatura. Georgia. U.S.S.R. Geol Soc Am Bull 96, 1398-1406.

Bonatti, E., Kraemer, T., Rydel. H. 1972. Classification and genesis of submarine iron–manganese deposits. In: Horn. D.R. (Ed.). Ferromanganese Deposits on the Ocean Floor. Washington. D. C.. Natl. Sci. Found. pp. 149–166.

Censi, P., Sprovieri, M., Larocca, D., Aricò, P., Saiano, F., Mazzola, S., Ferla, P. 2007. Alteration effects of volcanic ash in seawater: Anomalous Y/Ho ratios in coastal waters of the Central Mediterranean Sea. Geochem. Cosmochim. Acta 71 (22). 5405–5422.

Censi, P., Randazzo, L.A., Zuddas, P., Saiano, F., Aricò, P., Andò, S. 2010. Trace element behaviour in seawater during Etna's pyroclastic activity in 2001: concurrent effects of nutrients and formation of alteration minerals. J. Volcanol. Geotherm. Res. 193 (1–2). 106–116.

Censi, P., Inguaggiato, C., Chiavetta, S., Schembri, C., Sposito, F., Censi, V., Zuddas, P., 2017. The behaviour of zirconium. hafnium and rare earth elements during the crystallisation of halite and other salt minerals. Chem. Geol. 453. 80–91.

Censi, P., Sposito, F., Inguaggiato, C., Zuddas, P., Inguaggiato, S., Venturi, M., 2018. Zr, Hf and REE distribution in river water under different ionic strength conditions. Sci.Total Environ. 645, 837–853.

Censi, P., Raso, M, Saiano, F., Zuddas,P, Oliveri, E. 2019. Zr/Hf ratio and REE behaviour: A coupled indication of lithogenic input in marginal basins and deep-sea brines. Deep-Sea Res. Part II 164, 216-223.

Chakhmouradian, A.R., Wall, F. 2012. Rare earth elements: minerals, mines, magnets (and more). Elements 8, 333–342

Chen, S.. Yin, X.B., Wang, X.Y., Huang, X., Ma, Y., Guo, K., Zeng, Z.G. 2018. The geochemistry and formation of ferromanganese oxides on the eastern flank of the Gagua Ridge. Ore Geol. Rev., 95, 118-130

Choi, J.H., Hariya, Y., 1992. Geochemistry and depositional environment of Mn oxide deposites in the Tokora Belt, norteastern Hokkaido, Japan. Econ. Geol. 87, 1265–1274.

Crerar, D.A., Namson, J., Chyi, M.S., Williams, L., Feigenson, M.D., 1982. Manganiferous cherts of the Franciscan assemblage: I. General geology, ancient and modern analogues, and implications for the hydrothermal convection at oceanic spreading centers. Econ. Geol. 77, 519–540

Deng, X.H., Chen, Y.J., Yao, J.M., Bagas, L., Tang, H.S., 2014. Fluorite REE-Y (REY) geochemistry of the ca. 850 Ma Tumen molybdenite-fluorite deposit, eastern Qinling, China: constraints on ore genesis. Ore Geol. Rev. 63, 532–543

Dill, H.G., Hansen, B.T., Weber, B., 2011. REE contents, REE minerals and Sm/Nd isotopes of granite- and unconformity-related fluorite mineralization at the western edge of the Bohemian massif: with special reference to the Nabburg-Wölsendorf District, SE Germany. Ore Geol. Rev. 40, 132–148.

Dekov,V.M., Maynard, J.B., Kamenov, G.D., Rouxel, O., Lalonde, S., Juranov, S. 2020. Origin of the Oligocene manganese deposit at Obrochishte (Bulgaria): Insights from C, O, Fe, Sr, Nd, and Pb isotopes. *Ore Geology Reviews* (https://doi.org/10.1016/j.oregeorev.2020.103550).

Dosso, L., Hanan, B.B., Bougault, H., Schilling, J.G., and Joron, J.-L., 1991. Sr-Nd-Pb geochemical morphology between 10° and 17° N on the Mid-Atlantic Ridge: a new MORB isotope signature. *Earth Planet. Sci. Lett.*,106:29-43.

Dosso, L., Bougault, H., and Joron, J.L. 1993. Geochemical morphology of the North Atlantic Ridge, 10°-24°N: trace element-isotope complementarity. *Earth Planet. Sci. Lett.*, 120:443-462.

Dubinin, A.V. 2006. Rare Earth Elements in the Ocean. Nauka, Moscow (in Russian with English abstract).

Ehya, F. 2012. Variation of mineralizing fluids and fractionation of REE during the emplacement of the vein-type fluorite deposit at Bozijan, Markazi Province, Iran. J. Geochem. Explor. 112, 93–106.

Elderfield, H. 1988. The oceanic chemistry of the rare-earth elements. *Phil. Transac. Roy. Soc. London* A325, 105–126.

Firdaus, M. L., Minami T., Norisuye K. and Sohrin Y. 2011. Strong elemental fractionation of Zr–Hf and Nb–Ta across the Pacific Ocean. Nat. Geosci. 4, 227–230.

German, C.R., Elderfield, H., 1990. Application of the Ce anomaly as a paleoredox indicator: the ground rules. Paleoceanography 5, 823.

German, C.R., Holliday, B.P., Elderfield, H., 1991. Redox cycling of rare earth elements in the suboxic zone of the Black Sea. Geochim. Cosmochim. Acta 55, 3553–3558.

Godfrey, L.V., Mills, R., Elderfield, H., and Gurvich, E., 1994. Lead behaviour at TAG hydrothermal vent field, 26°N, Mid-Atlantic ridge. *Mar. Chem.*, 46:237-254.

Godfrey L.V., White, W.M., Salters, V J.M. 1996. Dissolved zirconium and hafnium distributions across a shelf break in the northeastern Atlantic Ocean. Geochim. Cosmochim. Acta 60, 3995–4006.

Godfrey, L.V., Zimmermann, B., Lee, D.C., King, R.L., Vervoort, J.D., Sherrell, R.M., Halliday, A.N. 2009. Hafnium and neodymium isotope variations in NE Atlantic seawater. Geochem.Geophys. Geosyst. 10, 1-13.

Gultekin AH. 1998. Mineralogical and chemical doses are used to determine the origins of manganese deposits. Geol Eng 50: 39-46.

Gultekin, A.H,, Balcı, N. 2018. Geochemical Characteristics of Sedimentary Manganese Deposit of Binkılıç, Trache Basin, Turkey. J Geol Geophys 7/3, 336.

Hamelin, B., Dupré, B., and Allègre, C.J., 1984. Lead-strontium isotopic variations along the East Pacific Rise and the Mid-Atlantic Ridge: a comparative study. *Earth Planet. Sci. Lett.*, 67:340-350.

Hart, S.R., 1984. A large-scale isotope anomaly in the Southern Hemisphere mantle. *Nature*, 309:753-757.

Hein, J.R., Koschinsky, A., Halbach, P., Manheim, F.T., Bau, M., Kang, J.-K., Lubik, N., 1997. Iron and manganese oxide mineralization in the Pacific. In: Nicholson, K., Hein, J.R., Bühn, B., Dasgupta, S. (Eds.), Manganese Mineralization: Geochemistry and Mineralogy of Terrestrial and Marine Deposits. 123–138.

Hein, J.R., Bolton, B. 1994. Formation of the Chiatura and Nikopol manganese carbonate ores, Georgia and Ukraine. Abstracts, Fermor Lecture Meeting, The Geological Society of London, 26-27 September, 1994, London, UK, p. 12.

Hein, J.R., Dowling, J., Stamatakis, M.G., 1999. HydrothermalMn-oxide deposit rich in Ba, Zn, As, Pb and Sb in Milos Island, Greece. In: Stanley, C.J. Ed. , Mineral Deposits: Processes toProcessing. A.A. Balkema, Rotterdam 519–522.

Hein, J.R., Stamatakis, M.G., Dowling, J. 2000. Trace metal-rich Quaternary hydrothermal manganese-oxide and barite deposit, Milos Island, Greece. Trans. Inst. Min. Metall.,Sect. B 109, 67–76.

Hein, J.R., Mizell, K., Koschinsky, A., Conrad, T.A., 2013. Deep-ocean mineral deposits as a source of critical metals for high- and green-technology applications: comparison with land-based resources. Ore Geol. Rev. 51, 1–14.

Hein, J.R., Koschinsky, A., 2014. Deep-ocean ferromanganese crusts and nodules. In: Holland, H.D., Turekian, K.K. (Eds.), Treatise on Geochemistry, second edition vol.13. Oxford, Elsevier, pp. 273–291.

Hein, J.R., Spinardi, F., Okamoto, N., Mizell, K., Thorburn, D., Tawake, A., 2015. Critical metals in manganese nodules from the Cook Islands EEZ, abundances and distributions. Ore Geol. Rev. 68, 97–116.

Hein, J.R. Konstantinova, N., Mikesell, M., Mizell, K., Fitzsimmons, J.N., Lam, P.J. , Jensen, L.T., Xiang, Y., Gartman, A., Cherkashov, G., Hutchinson, D.R., Till, C.P. 2017. Arctic deep water ferromanganese-oxide deposits reflect the unique characteristics of the Arctic Ocean. Geochem. Geophys. Geosyst., 18, 3771-3800.

Ito, E., White, W.M., and Göpel, C., 1987. The O, Sr, Nd and Pb isotope geochemistry of MORB. *Chem. Geol.*, 62:157-176.

James, R., Elderfield, H., Palmer, M., 1995. The chemistry of hydrothermal fluids from the Broken Spur site, 29°N Mid-Atlantic Ridge. Geochim. Cosmochim. Acta 59, 651–659

Josso, P., Pelleter, E., Pourret, O., Fouquet, Y., Etoubleaua, J., Cheron, S., Bollinger, C., 2017. A new discrimination scheme for oceanic ferromanganese deposits using high field strength and rare earth elements. Ore Geol. Rev. 87, 3–15.

Khamkhadze, N.I. 1982. Oligocene tectonic hydrothermal activity of districts with siliceous-manganese sediments in Georgia. VI I AGOD Symposium, Collected Abstracts, Tbilisi, 292-293.

Khamkhadze, N.I. 1984. On the relationship of silica and ore formation in manganese deposits in Georgia, USSR. In: G. Morvai (ed.) Geology and Geochemistry of Manganese, Budapest, Hungarian Acad. Sci. Publ., 427-431.

Koç, S., Özmen, Ö., Öksüz, N., 2000. Kasımağa (Keskin-Kırıkkale) mangan oksit cevherleşmesinin oluşum ortamını tanımlayan jeokimyasal özellikler. Maden Tetkik ve Arama (MTA) Dergisi 122, 107–118.

Konstantinova, N., Cherkashov, G., Hein, J. R., Mirão, J., Dias, L., Madureira, P., & Kuznetsov, V., 2017. Composition and characteristics of the ferromanganese crusts from the western Arctic Ocean. Ore Geology Reviews, 87, 88–99.

Kuleshov, V.N. 2003. Isotopic composition (δ13C. δ18O) and the origin of manganese carbonate ores from the Early Oligocene deposits, the Eastern Paratethys: Chemie der Erde 63, 329–363.

Kuleshov, V.N. Brusnitsyn, A.I. 2005. Isotopic composition (δ13C. δ18O) and the origins of carbonates from manganese deposits of the southern Urals: Lithology and Mineral Resources 40, 364–375.

Kuleshov, V.N., Bych, A.F., 2002. Isotopic composition (δ^{13}C. δ^{18}O) and the origin of manganese carbonate ores of the Usa Deposit (Kuznetskii Alatau): Lithology and Mineral Resources 37, 330–343.

Loizeau, J.L., Span, D., Coppee, V., Dominik, J. 2001. Evolution of the trophic state of Lake Annecy (eastern France) since the last glaciation as indicated by iron. manganese and phosphorus speciation. Journal of Paleolimnology 25, 205–214

Maynard, J. B., 1983. Geochemistry of sedimentary ore deposits: New York, Heidelberg, Berlin, Springer-Verlag, p. 121-144.

Maynard , J.B. 2010. The chemistry of manganese ores throughtime: a signal of increasing diversity of earth-surface environ-ments. Econ. Geol.105, 535–552.

Mazumdar, A., Tanaka, K., Takahashi, T., Kawabe, I., 2003. Characteristics of rare earth element abundances in shallow marine continental platform carbonates of Late Neoproterozoic successions from India. Geochem. J. 37, 277–289

McLennan, S.M., 1989. Rare earth elements in sedimentary rocks; influence of provenance and sedimentary processes. Rev. Mineral. Geochem. 21, 169–200.

Mills, R., Elderfield, H., and Thompson, J., 1993. A dual origin for the hydrothermal component in a metalliferous sediment core from the Mid-Atlantic Ridge. *J. Geophys. Res.*, 98:9671-9681.

Muiños, S.B., Frank, M., Maden, C., Hein, J.R., van de Flierdt, T., Lebreiro, S.M., Gaspar, L.,Monteiro, J.H., Halliday, A.N., 2008.New constraints on the Pb and Nd isotopic evolu-tion of NE Atlantic water masses. Geochemistry, Geophysics, Geosystems 9, 18.

Naeher S, Gilli A, North R, Hamann Y, Schubert C. 2013. Tracing bottom water oxygenation withsedimentary Mn/Fe ratios in Lake Zurich, Switzerland. Chem Geol 352, 125–33.

Nicholson, K. 1992. Contrasting mineralogical-geochemical signatures of manganese oxides: guides to metallogenesis. Econ. Geol. 87, 1253–1264.

Okay, A.I., Simmons, M., Özcan, E., Starkie, S., Bidgood, M. & Kylander-Clark, A.R.C., 2020, Eocene-Oligocene succession at Kıyıköy (Midye) on the Black Sea coast in Thrace. Turkish Journal of Earth Sciences, 29, 139-153.

Oygür, V., 1990. Çayırlı (Ankara-Haymana) manganez yatağının jeolojisi ve kökeni üzerine görüşler. Maden Tetkik ve Arama Genel Müdürlüğü (MTA) Dergisi 110, 29–44.

Roy, S., 1981, Manganese deposits: New York, Academic Press, 451 p.

Roy A, Chakrabarti G, Shome D. 2018. Geochemistry of the Neoproterozoic Narji limestone, Cuddapah Basin, Andhra Pradesh, India: implication on palaeoenvironment. Arab J Geosci 11, 784–796

Sasmaz, A., Turkyılmaz, B., Ozturk, N., Yavuz, F., Kumral, M., 2014. Geology and geochemistry of Middle Eocene Maden complex ferromanganese deposits from the Elazığ-Malatya region, eastern Turkey. Ore Geol. Rev. 56, 352–372.

Sasmaz, A., Kryuchenko, N., Zhovinsky, E., Suyarko, V., Konakci, N., Akgul, B. 2018. Major, trace and rare earth element (REE) geochemistry of different colored fluorites in the Bobrynets region, Ukraine. Ore Geology Reviews 102, 338-350.

Schmidt, K., Bau, M., Hein, J.R., Koschinsky, A. 2014**.** Fractionation of the geochemical twins Zr/Hf and Nb/Ta during scavenging from sea water by hydrogenetic ferromanganese crusts. Geochim. Cosmochim. Acta, 140, 468-487

Schwinn, G., Markl, G. 2005. REE systematics in hydrothermal fluorite. Chem. Geol. 216, 225–248.

Sinanoglu, D., Sasmaz, A. 2019. Geochemical evidence on the depositional environment of Nummulites accumulations around Elazig, Sivas, and Eskişehir (Turkey) in the middle Eocene sub-epoch. Arabian J. Geoscie. 12:759.

Slack, J., Grenne, T., Bekker, A., Rouxel, O., Lindberg, P., 2007. Suboxic deep seawater in the late Paleoproterozoic: evidence from hematitic chert and iron formation related to seafloor hydrothermal sulfide deposits, central Arizona, USA. Earth Planet. Sci. Lett. 255, 243–256.

Sokal, R.R. Rohlf, F.J. 1995. Biometry: The Principles and Practice of Statistics in Biological Research, third ed.. W.H. Freeman and Co, New York, p 887.

Soyol-Erdene, T.-O., Huh, Y., 2013. Rare earth element cycling in the pore waters of the Bering Sea Slope (IODP Exp. 323). Chem. Geol. 358, 75–89.

Strishkov, V., Levine, R.M. 1987. The Manganese Industry of the U.S.S.R. Washington, DC: U. S. Bureau of Mines/U. S. Government Printing Office.

Sun, S.-S., 1980. Lead isotopic study of young volcanic rocks from midocean ridges, ocean islands and island arcs. *Philos. Trans. R. Soc. London A*, 297:409-445.

Strishkov, V., Levine, R.M. 1987. The manganese industry of the U.S.S.R. Washington, DC. U.U. Bureau of Mines/U.S. Government Printing Office.

Takahashi, Y., Hirata, T., Shimizu, H., Ozaki, T., Fortin, D., 2007. A rare earth element signature of bacteria in natural waters? Chem. Geol. 244, 569–583.

Taylor S. R. and McLennan S. M. 1985. The Continental Crust: Its Composition and Evolution. Blackwell, Oxford.

Tobia, F.H. 2018. Stable isotope and rare earth element geochemistry of the Baluti carbonates (Upper Triassic), Northern Iraq. Geosci J 22 (6), 975–987

Tostevin, R., Shields, G.A., Tarbuck, G.M., He, T., Clarkson, M.O., Wood, R.A., 2016. Effective use of the cerium anomalies as a redox proxy in carbonate-dominated marine settings. Chem. Geol 438, 146–162.

Toth, J.R., 1980. Deposition of submarine crusts rich in manganese and iron. Geol. Soc.Am. Bull. 91, 44–54.

Turekian, K.K., Wedepohl, K.H. 1961. Distribution of elements in some major units of earth's crust. Geol Soc Am Bull 72, 175–192.

Varentsov, I. M., and Rakhmanov, V. P., 1980. Manganese deposits of the USSR (A review), *in* Varentsov, I. M., and Grasselly, Gy., eds., Geology 319-391

Varentsov, I.M. 2002. Genesis of the eastern Paratethys manganese ore giants. Impact of events at the Eocene/Oligocene boundary. Ore Geol Rev 20, 65-82.

Varentsov, I.M.. Muzyliov, N.G., Nikolaev, V.G., Stupin, S.I. 2003. The origin of black shale-hosted Mn deposits in Paratethyan basins: constraints from geological events at the Eocene/Oligocene boundary. Russian Journal of Earth Sciences 5, 255-272.

Vereshchagin, O. S., Perova, E. N., Brusnitsyn, A. I., Ershova, V. B., Khudoley, A. K., Shilovskikh, V. V., Molchanova, E.V. 2019. Ferro-manganese nodules from the Kara Sea: mineralogy, geochemistry and genesis. *Ore Geol. Rev.* 106, 192–204.

von Blanckenburg, F., O'Nions, R.K., Hein, J.R. 1996. Distribution and sources of pre-anthropogenic lead isotopes in deep ocean water from Fe-Mn crusts, Geochim. Cosmochim. Acta, 60, 4936– 4957,

von Blackenburg, F., Nägler, T.F., 2001. Weathering versus circulation-controlledchanges in radiogenic isotope tracer composition of the Labrador Sea and northAtlantic deep water. Paleoceanography 16, 424–434

Wang, C.M., Deng, J., Carranza, E.J.M., Lai, X.R., 2014. Nature, diversity and temporal–spatial distributions of sediment-hosted Pb–Zn deposits in China. Ore Geol. Rev. 56, 327–351

Zeng, Z., Ouyang, H., Yin, X., Chen, S., Wang, X., Wua, L., 2012. Formation of Fe–Si–Mn oxyhydroxides at the PACMANUS hydrothermal field, Eastern Manus Basin: mineralogical and geochemical evidence. J. Asian Earth Sci. 60, 130–146.

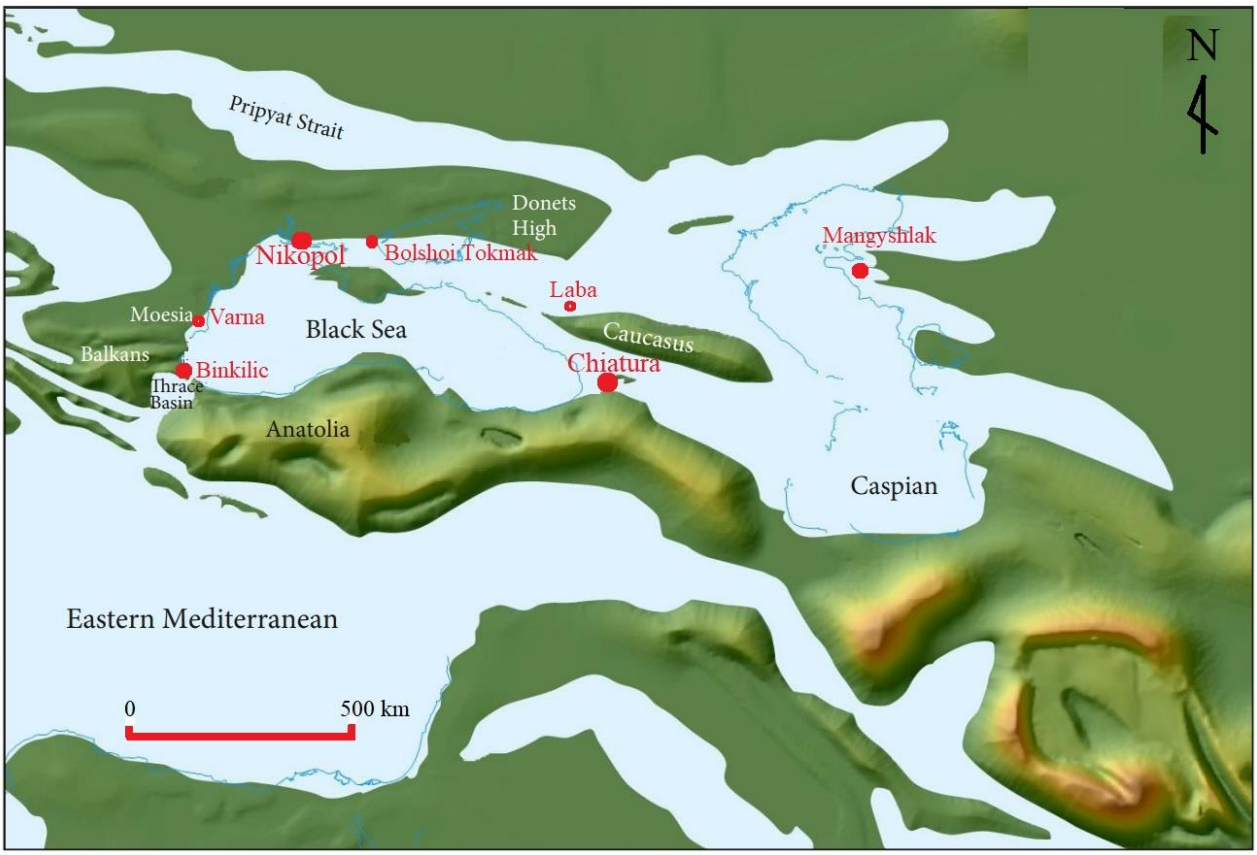

Fig. 1. Map showing location of Chiatura and other Oligocene manganese deposits and simplified regional palaeogeographic setting of the early Oligocene of the eastern Paratethys (modified from Okay et al., 2020).

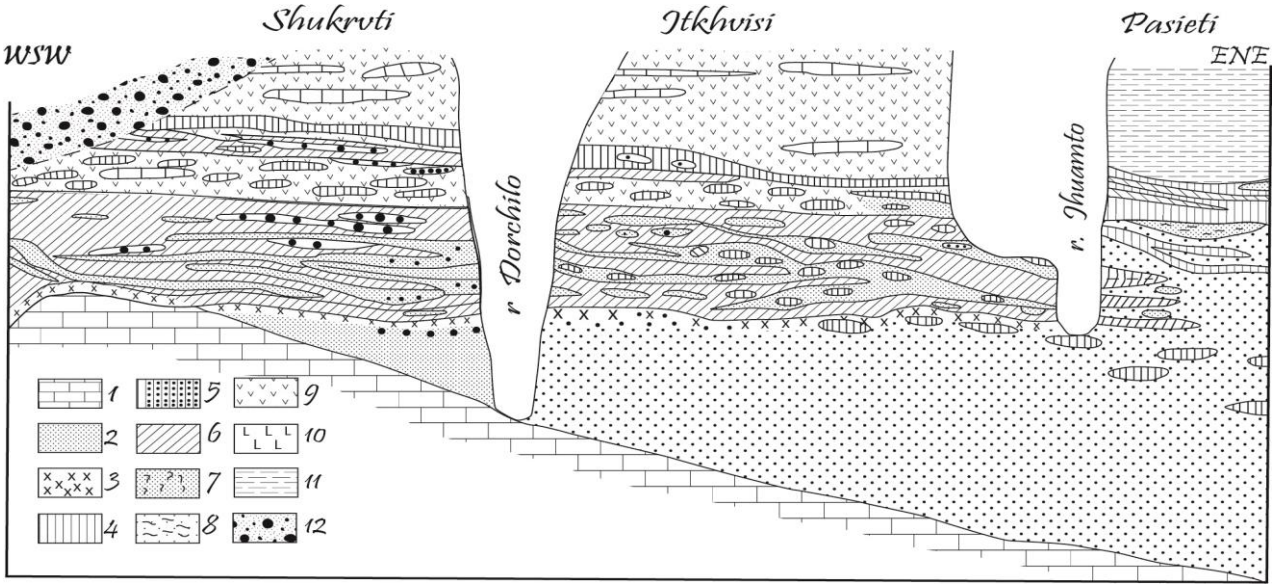

Fig. 2. Geological section of the Chiatura manganese deposit; 1- Late Cretaceous limestone; 2- early Oligocene sandstone; 3- phosphorite; 4- carbonate ore; 5 - hydroxide ores; 6- oxide ores; 7- Mn-bearing sandstone and siltstone; 8 – claystone with Fe-montmorillonite-glauconite; 9 - bentonite-zeolite; 10 - spongolite; 11- Maikope terrigenous siltstone and claystone; 12 - Miocene arkose sandstone

Fig. 3. Oxide-hydroxide ores in field

Fig. 4. Oxide-hydroxide ores in upper zone of manganese deposit

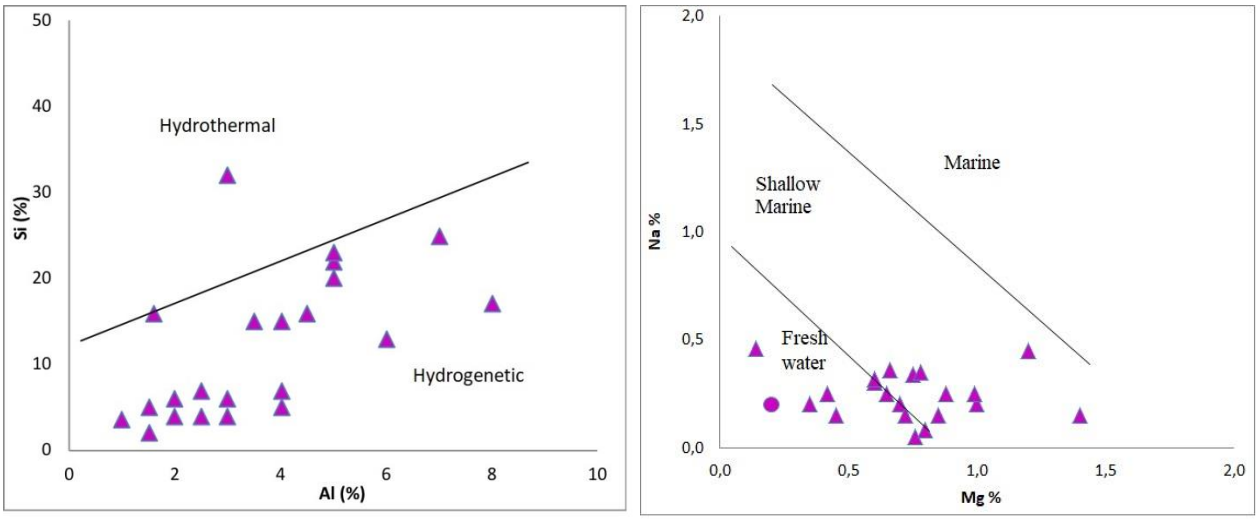

Fig. 5. Al-Si and Mg-Na discrimination diagrams for the Chiatura manganese oxides after Choi and Hariya (1992) and Nicholson (1992).

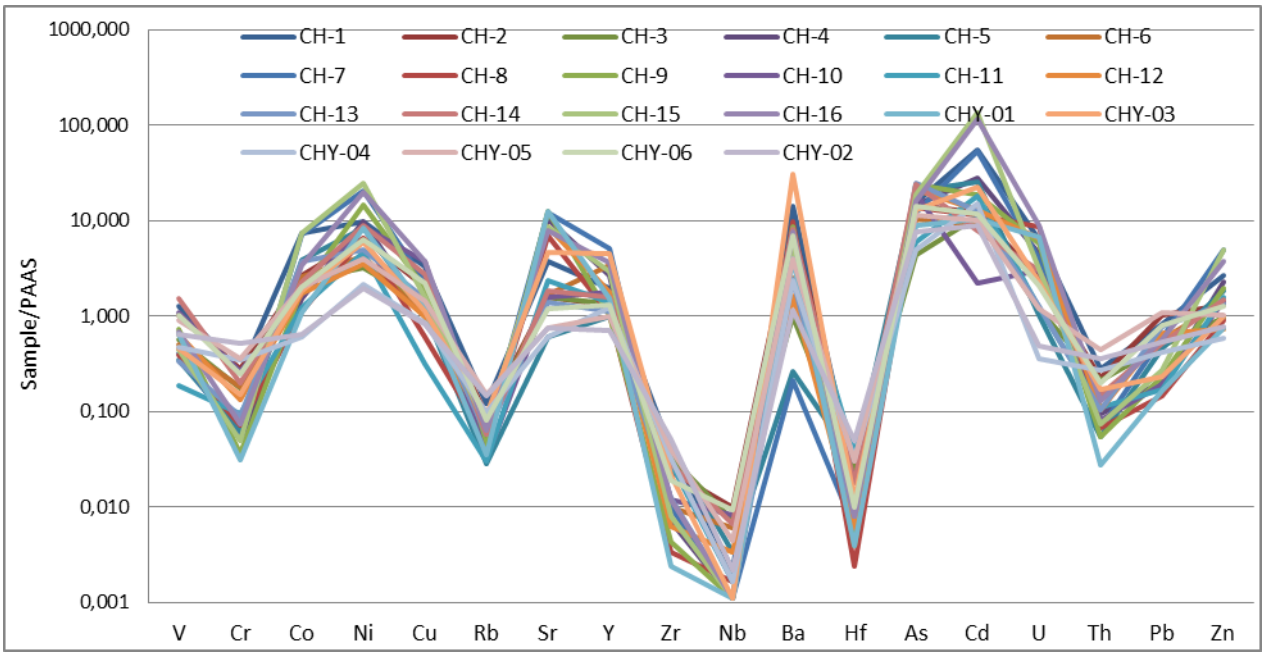

Fig. 6. Post Archean Australian Shale (PAAS)-normalized trace element distribution of Chiatura manganese oxides; PAAS data from Taylor and McLennan (1985).

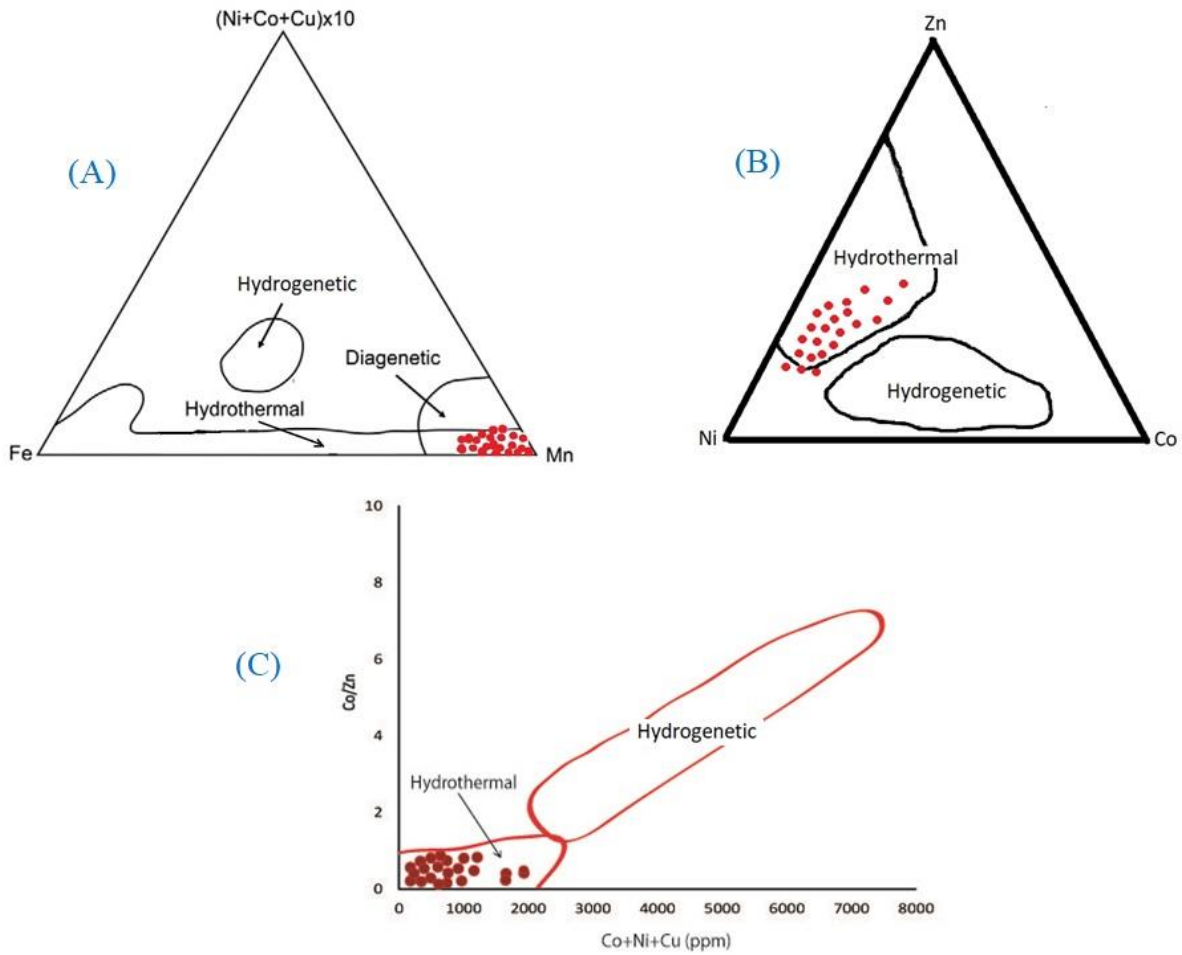

Fig. 7. Different discrimination diagrams for Chiatura manganese oxides. (A) Mn–Fe–(Ni + Co + Cu)x10 diagram (after Bonatti et al., 1972; Crerar et al., 1982), (B) Ni–Zn–Co diagram (after Choi and Hariya, 1992), (C) Co/Zn–(Co + Ni + Cu) diagram (after Toth, 1980); all indicate a predominantly hydrothermal origin.

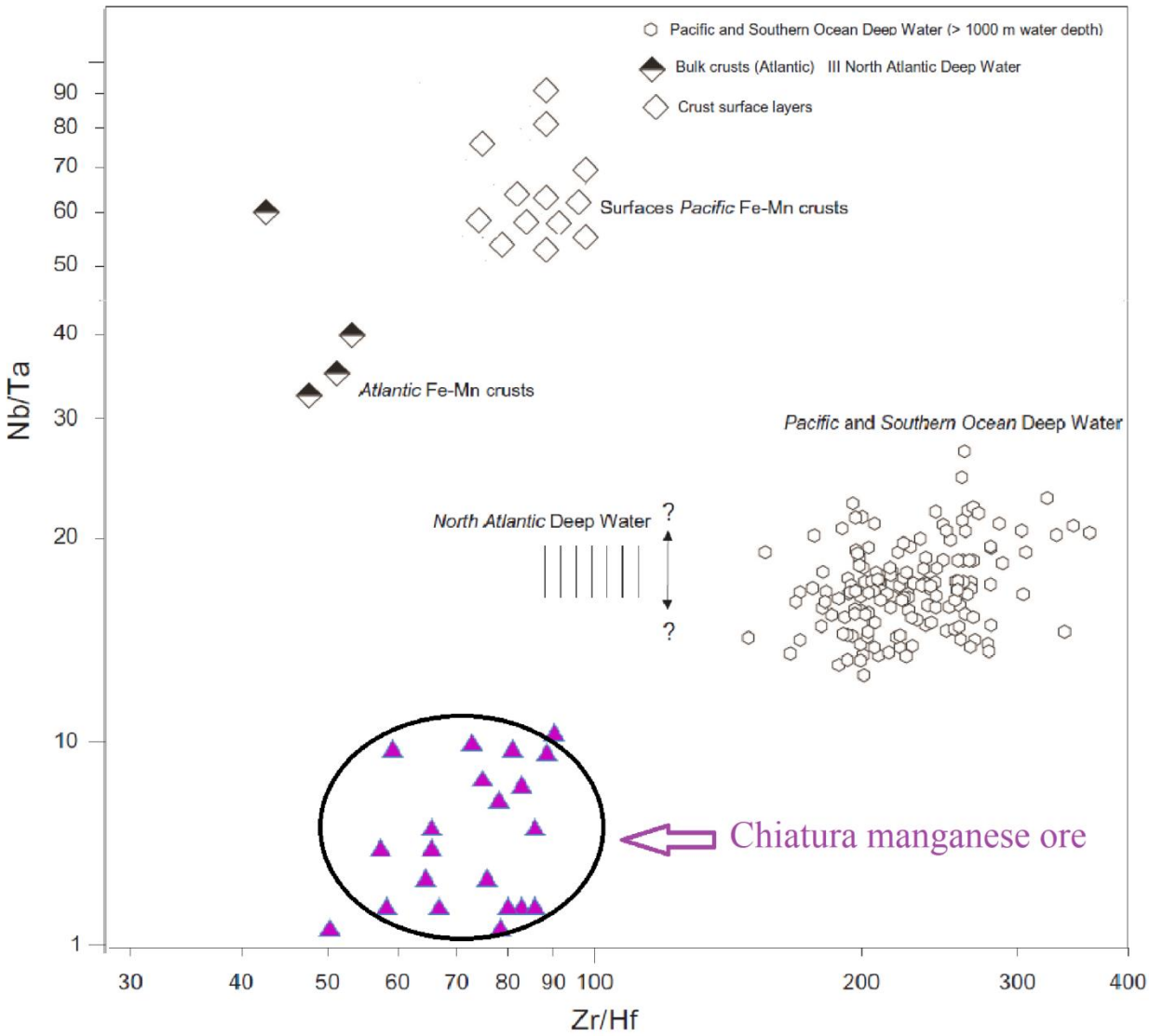

Fig. 8. Zr/Hf and Nb/Ta ratios in Chiatura manganese oxides compared to other oxide deposits (modified from Schmidt et al., 2014; North Atlantic Deep Water: Godfrey et al., 1996, 2009; Arctic and Pacific Deep Water: Firdaus et al., 2011)

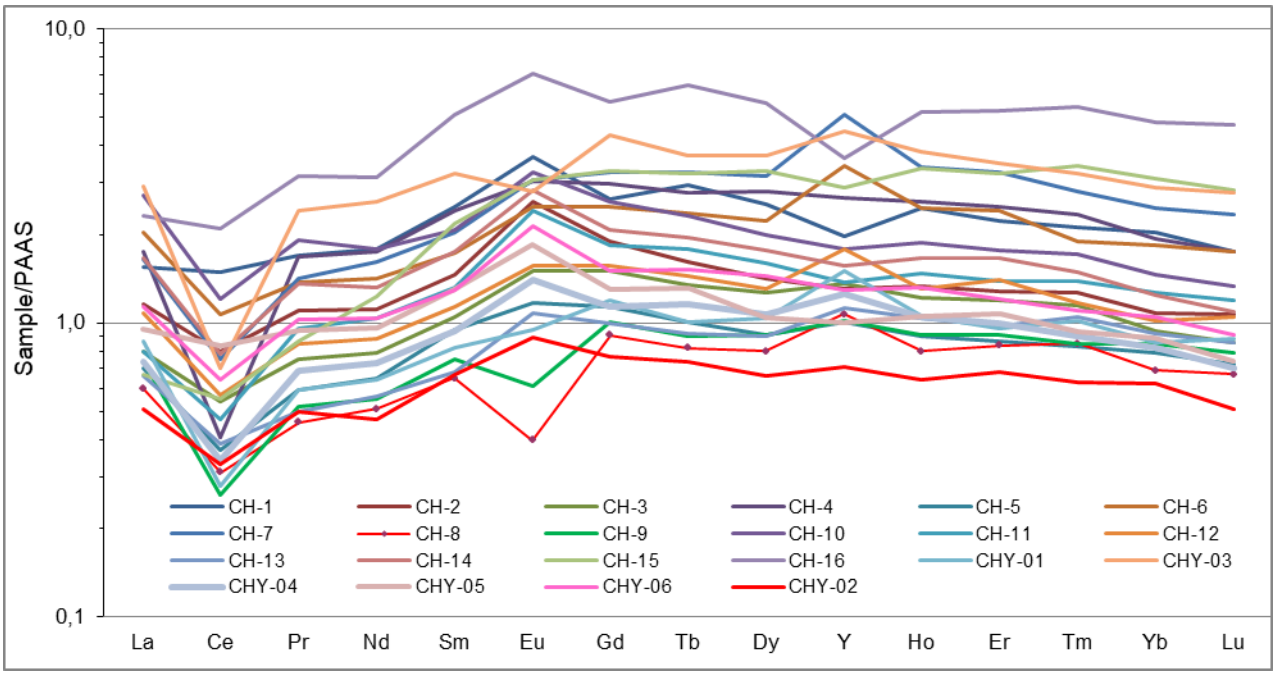

Fig. 9. PAAS-normalized REE + Y patterns of the Chiatura manganese samples; PAAS from Taylor and McLennan (1985).

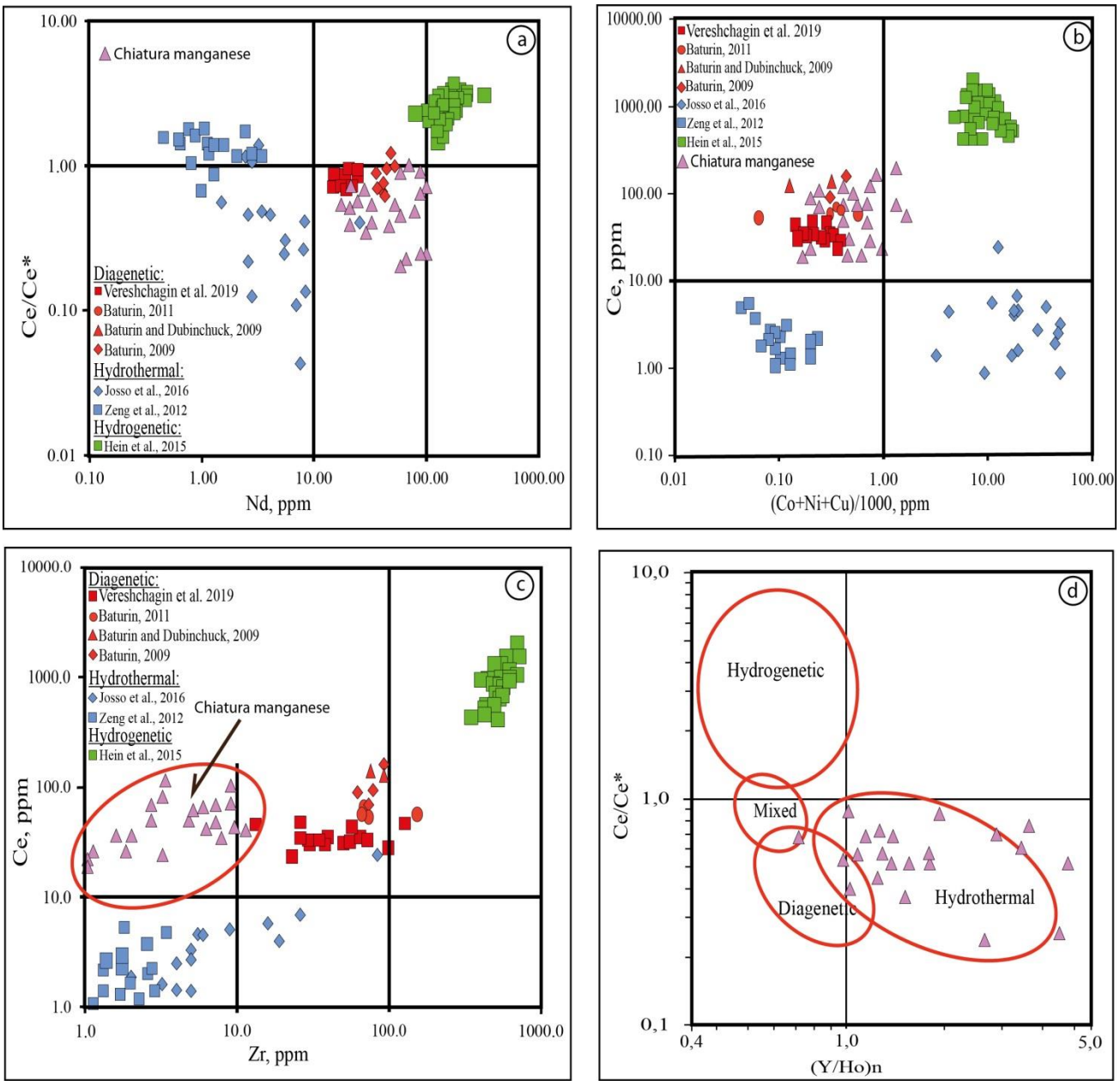

Fig. 10. Different genetic types of Mn-oxide deposits: a) Ce/Ce* ratio *vs* Nd concentration (after Bau et al., 2014); b) Ce vs Co+Ni+Co)/1000 ratios (after Vereshchagin et al., 2019); c) Ce vs Zr ratios (after Vereshchagin et al., 2019); and d) Ce/Ce* vs $(Y/Ho)_n$ diagram (after Bau et al., 2014; data from this study only). The ferromanganese concretions/nodules in the Kara Sea from Baturin (2011) and Vereshchagin et al. (2019); ferromanganese nodules in the Gulf of Finland, Baltic Sea from Baturin (2009); ferromanganese nodules from Riga Bay from Baturin and Dubinchuk (2009).

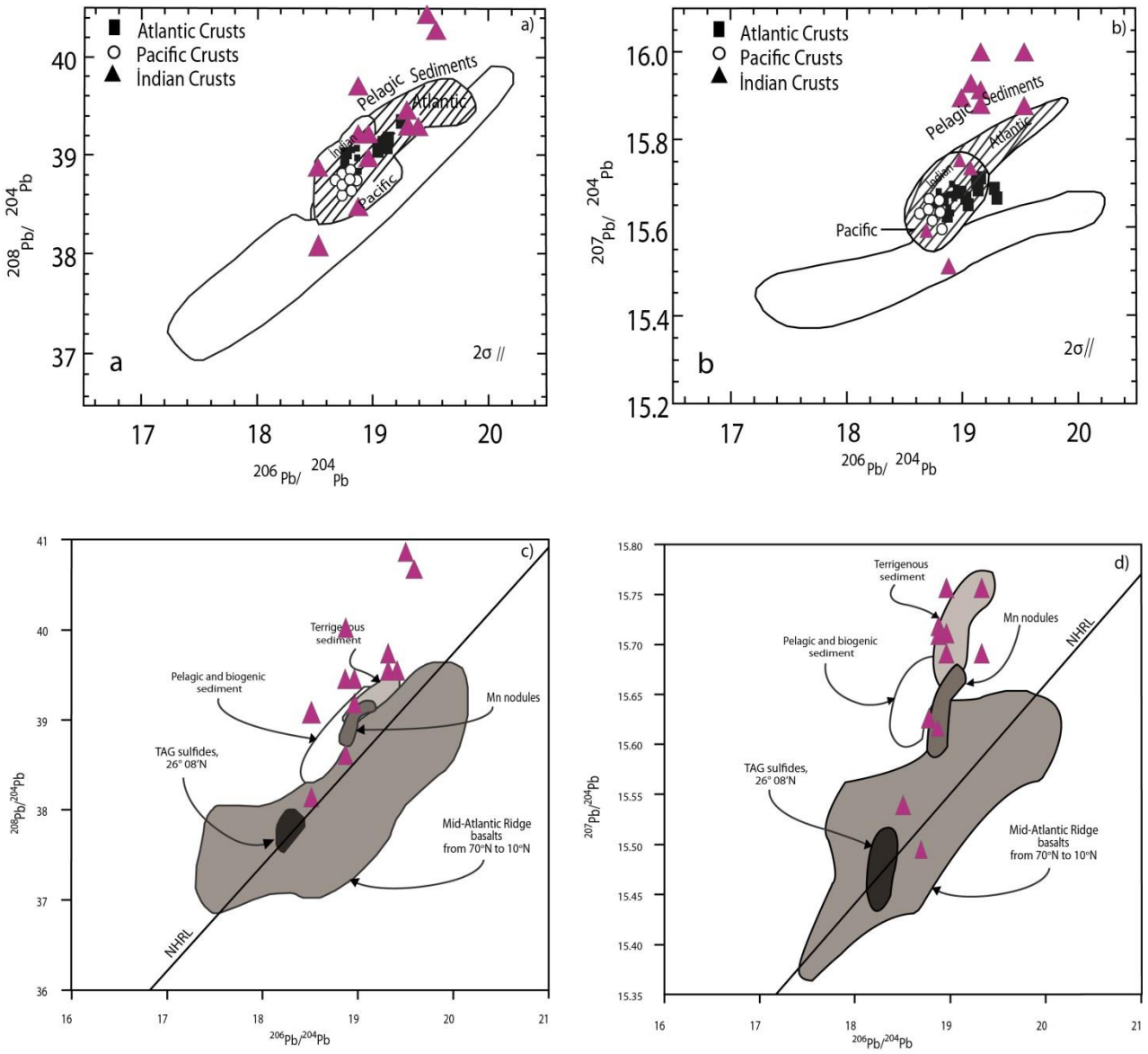

Fig. 11. a and b) Comparison of Pb isotope compositions for Chiatura samples (red triangles) with MORB, pelagic sediments, and Fe-Mn crusts (taken from von Blanckenburg et al., 1996); c and d) Pb isotopes for Chiatura samples (red triangles) compared with Mid-Atlantic Ridge basalt (Sun, 1980; Hamelin et al., 1984; Ito et al., 1987; Dosso et al., 1991, 1993); Atlantic sediments (Ben Othman et al., 1989); TAG sulphides (Ito et al., 1987; Dosso et al., 1993); Mn nodules (Ben Othman et al., 1989; Mills et al., 1993; Godfrey et al., 1994). NHRL = the Northern Hemisphere Reference Line of Hart (1984) (after Andrieu et al., 1998).

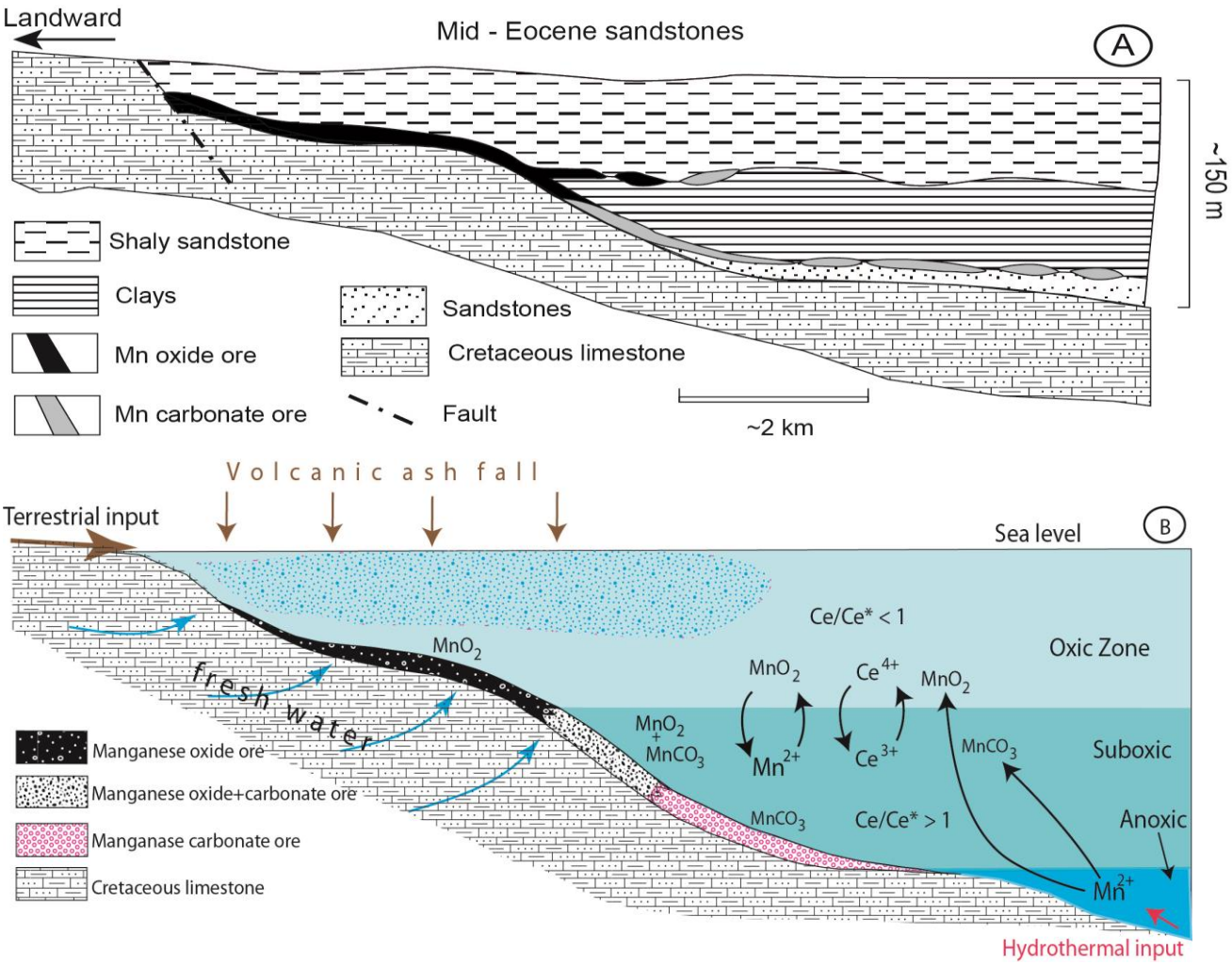

Fig. 12. A: Schematic cross section of the Chiatura manganese deposits (after Bolton and Frakes and 1985), B; Genetic model of Chiatura manganese ores presented here; ash falls occurred only occasionally.

Table 1. Major oxide contents (wt. %) of Chiatura manganese-oxide deposit.

	MnO	SiO_2	Al_2O_3	Fe_2O_3	MgO	CaO	Na_2O	K_2O	TiO_2	P_2O_5	LOI	Sum
CH-1	23,1	42,1	9,56	4,67	1,13	1,43	0,37	1,59	0,35	0,37	14,0	98,7
CH-2	20,1	48,7	9,29	3,82	0,82	1,37	0,39	1,53	0,39	0,43	12,4	99,3
CH-3	20,2	38,8	8,11	2,85	1,54	4,93	0,55	1,57	0,33	0,64	20,3	99,8
CH-4	55,4	9,00	5,14	1,46	1,07	4,08	0,43	0,79	0,09	0,28	22,2	99,9
CH-5	48,0	7,12	1,73	1,04	1,69	7,86	0,08	0,27	0,07	0,28	30,6	98,8
CH-6	25,8	31,1	6,28	2,27	1,72	7,17	0,49	1,15	0,24	1,93	21,5	99,7
CH-7	54,1	8,45	2,93	1,31	1,29	4,27	0,40	0,70	0,09	0,32	25,2	99,1
CH-8	51,5	9,80	2,36	0,93	1,01	6,70	0,51	0,70	0,08	1,03	24,9	99,5
CH-9	53,7	7,30	4,11	0,93	1,15	6,56	0,58	0,57	0,06	0,32	23,3	98,6
CH-10	40,7	33,1	3,33	1,49	0,30	1,49	0,31	1,01	0,07	0,83	15,1	97,7
CH-11	7,62	77,0	6,10	0,89	0,20	0,58	0,62	2,36	0,08	0,28	3,7	99,5
CH-12	44,5	15,2	4,53	1,58	1,23	7,61	0,35	0,85	0,13	1,56	21,6	99,1
CH-13	49,5	14,1	3,57	1,97	1,29	4,90	0,20	1,09	0,16	0,39	22,1	99,3
CH-14	41,4	30,0	6,54	3,99	0,62	0,97	0,28	0,97	0,20	0,39	13,6	99,0
CH-15	49,1	12,2	7,14	1,98	1,73	3,74	0,58	0,80	0,10	0,27	22,2	99,8
CH-16	47,6	15,3	7,64	2,32	1,14	2,26	0,27	0,84	0,17	0,24	21,5	99,2
CHY-1	58,9	4,88	2,82	2,59	0,75	6,24	0,23	0,66	0,05	1,30	21,5	99,4
CHY-3	50,9	14,3	5,08	2,20	1,28	2,45	0,23	0,78	0,19	0,16	20,7	98,3
CHY-4	4,35	28,6	11,6	4,43	1,17	21,7	0,08	0,75	0,35	0,03	26,6	99,7
CHY-5	11,5	52,9	13,2	5,43	1,04	1,12	0,46	1,67	0,71	0,11	11,5	99,6
CHY-6	21,6	51,1	8,48	3,26	0,71	1,14	0,41	1,66	0,34	0,37	10,7	99,4
CHY-2	3,87	37,7	14,8	5,91	1,39	12,6	0,12	1,02	0,46	0,04	22,0	99,8
Average	**35,5**	**26,8**	**6,56**	**2,61**	**1,10**	**5,05**	**0,36**	**1,06**	**0,21**	**0,53**	**19,4**	99,1
PAAS	**7.22**	**62.8**	**18.9**	**0.11**	**1.30**	**2.20**	**1.20**	**3.70**	**0.99**	**0.16**	**-**	98.6

Table 2: Trace element concentrations (ppm) and lead isotope ratios of Chiatura manganese deposit samples.

	V	Cr	Co	Ni	Cu	Rb	Sr	Y	Zr	Nb	Ba	Hf	As	Cd	U	Th	Pb	Zn	Mn:Fe	Co:Zn	Co:Ni	Co+Ni+Cu	Zr:Hf	Nb/Ta	208Pb	207Pb	206Pb	204Pb	208Pb/204Pb	207Pb/204Pb	206Pb/204Pb
CH-1	179	26	147	584	167	19.2	746	53.1	8.3	0.04	9026	0.11	26	5.6	19	4.1	17	227	6.2	0.65	0.25	898	75	48	8.60	3.50	4.14	0.21	41.0	16.7	19.7
CH-2	144	28	52.9	388	102	14.7	313	35.5	4.9	0.18	5246	0.14	25	1.2	7.7	3.3	21	112	6.5	0.47	0.14	543	35	34.8	10.7	4.45	5.30	0.27	39.6	16.5	19.6
CH-3	80	18	47.5	191	67	13.2	312	36.7	7	0.13	632	0.13	7	1.1	3.7	3.1	10	81	9.5	0.59	0.25	305	54	39.7	5.21	2.07	2.47	0.13	40.1	15.9	19.0
CH-4	65	5.1	30.8	584	52.9	7.9	2056	71.7	1.5	0.02	2906	0.02	25	2.8	14	1.4	4	194	35	0.16	0.05	668	75	44.9	<0.01	1.82	2.24	0.11	nd	16.5	20.4
CH-5	48	6.2	77.8	497	56	4.5	121	27.1	9.3	0.06	170	0.15	35	2.6	3.2	0.8	9	157	39	0.49	0.16	631	62	43.9	4.75	1.92	2.34	0.12	39.6	16.0	19.5
CH-6	70	18	51.7	255	50	11.6	338	92.4	2.1	0.11	1622	0.03	18	0.9	7.6	2	11	117	15	0.44	0.2	357	70	30.3	5.97	2.38	2.93	0.15	39.8	15.9	19.5
CH-7	57	5.2	143	1213	115	9.7	2455	137.3	2.1	<0.02	133	0.03	20	5.3	13	1	12	418	38	0.34	0.12	1472	70	31.2	6.26	2.49	2.98	0.16	39.1	15.6	18.6
CH-8	55	7.3	22.5	394	30	8.3	1411	28.8	0.7	0.03	6304	0.01	23	1.1	27	1	2.9	78	43	0.29	0.06	446	58	28.4	<0.01	1.28	1.53	0.08	nd	16.0	19.1
CH-9	101	3.6	37.9	871	97	7.1	2474	27.5	0.9	<0.02	5423	0.02	41	1.9	18	0.8	4.6	166	47	0.23	0.04	1006	45	25.9	<0.01	2.03	2.44	0.12	nd	16.9	20.3
CH-10	151	26	33.9	521	190	5.2	314	48.4	2.5	0.15	4879	0.03	33	0.2	9.5	1.2	3.9	122	26	0.28	0.07	745	83	29.9	2.04	0.83	0.99	0.05	40.8	16.6	19.8
CH-11	26	9.5	24.6	279	16	4.9	468	37.4	5.9	0.03	3441	0.18	10	1.8	3.8	1.6	3.4	135	10	0.18	0.09	320	33	23.1	1.80	0.71	0.83	0.05	36.0	14.2	16.6
CH-12	89	13	35	212	49	11.2	1752	47.9	1.3	0.06	1048	0.03	36	1.3	20	1.5	13	63	32	0.56	0.17	296	43	30	6.85	2.80	3.34	0.18	38.1	15.6	18.6
CH-13	47	9	74.6	296	76	9.3	279	30.4	2.6	0.02	1544	0.04	42	1.2	3.9	1.5	16	115	30	0.65	0.25	447	65	34	8.11	3.34	4.00	0.21	38.6	15.9	19.0
CH-14	213	20	46.1	530	135	9.4	366	42.2	6	0.12	5207	0.09	41	0.8	9.5	2.2	10	127	12	0.36	0.09	712	67	19.9	5.49	2.15	2.59	0.13	42.2	16.5	19.9
CH-15	62	4.9	150	1489	79	11.6	1728	78.3	1.7	<0.02	3124	0.05	31	13	9.8	1.1	5.4	421	50	0.36	0.1	1717	34	27.9	<0.01	2.36	2.84	0.15	nd	15.7	18.9
CH-16	96	7.5	67.4	1212	186	10.3	1596	98.2	2.5	0.02	4855	0.04	27	11	28	1.9	11	317	24	0.21	0.06	1466	63	53	5.92	2.38	2.86	0.15	39.5	15.9	19.1
CHY-1	89	3.1	21.5	498	60	5.6	2506	40.8	0.5	<0.02	2516	0.02	15	1.1	21	0.4	3.3	63	63	0.34	0.04	579	25	29.2	<0.01	1.46	1.73	0.09	nd	16.2	19.2
CHY-3	65	15	36.8	361	56	14.9	922	121	4.5	<0.02	19524	0.06	22	2.2	7	2.5	4.7	84	25	0.44	0.1	454	75	33.3	<0.01	2.06	2.51	0.14	nd	14.7	17.9
CHY-4	67	35	12	130	43	15.8	120	33.6	6.7	0.03	1514	0.16	8	1.5	1.1	4	8.4	50	1.6	0.24	0.09	185	42	35.7	4.47	1.75	2.09	0.11	40.6	15.9	19.0
CHY-5	127	36	40.8	242	72	24.1	152	26.9	8.5	0.08	2532	0.15	19	1	3.7	6.5	22	88	2.7	0.47	0.17	355	57	19.7	11.46	4.64	5.64	0.30	38.2	15.5	18.8
CHY-6	143	25	40.7	375	112	13.1	242	34.9	4	0.17	4370	0.05	24	1.2	6.5	2.9	16	107	8	0.38	0.11	528	80	33.2	8.23	3.34	4.02	0.21	39.2	15.9	19.1
CHY-2	91	52	12.9	117	42	23.3	149	19	10.8	0.04	741	0.25	13	0.9	1.5	5.3	11	66	0.9	0.2	0.11	172	43	21.2	5.53	2.20	2.66	0.14	39.5	15.7	19.0
Ave.	**94**	**15**	**57**	**530**	**86**	**11**	**984**	**54.8**	**4.3**	**0.08**	**4096**	**0.07**	**25**	**2.9**	**11**	**2.1**	**9.9**	**154**	**24**	**0.37**	**0.11**	**650**	**57**	**33**	**6.34**	**2.36**	**2.84**	**0.15**	39.5	15.9	19.1

PAAS	140	100	20	60	50	160	200	27	210	18	636	5	1.7	0.1	3.1	15	20	85	--	--	--	--	--	--	--	--	--	--	--	--	--

Dash – means no data

Table 3. Major and trace element contents of various types of manganese deposits. Analyses taken from (1: Shah and Moon, 2007; 2-5: Choi and Hariya, 1992; 6: Gultekin and Balcı, 2018; 7: Oygür, 1990; 8: Koç et al., 2000; 9: Sasmaz et al., 2014).

Countries	Pakistan (1)	Japan (2)	Japan (3)	Japan (4)	Japan (5)	Turkey (6)	Turkey (7)	Turkey (8)	Turkey (9)	This study
Regions	Hazara	Wakasa	Koryu	Hinode	Tokora	Binkılıç	Çayırlı	Kasımağa	Elazig/Malatya	Chiatura
Origins	Hydrothermal/ hydrogenous	Hydrothermal	Hydrothermal	Sedimentary	Sedimentary	Sedimentary	Volcano-sedimentary	Volcano-sedimentary	Sedimentary exhalative	Sedimentary
SiO_2 (%)	9.41	58.16	40.56	12.7	32	9.69	63	13.4	24.6	26.3
TiO_2 (%)	0.84	0.04	0.05	0.04	0.91	0.30	0.03	0.10	0.14	0.21
Al_2O_3 (%)	12.5	0.55	0.63	1.27	8.82	1.39	0.65	2.95	3.62	6.56
Fe_2O_3 (%)	20.3	0.92	0.55	0.59	38.3	3.69	0.68	14	33.7	2.61
MnO (%)	33.78	32.5	42.06	67.2	5.22	53.2	29.2	40	11.6	35.6
MgO (%)	0.59	0.19	0.02	0.08	4.04	1.12	0.2	12.7	1.23	1.10
CaO (%)	6.43	4.15	1.65	1.67	8.82	16.6	0.24	6.82	9.78	5.05
Na_2O (%)	0.07	0.04	0.11	0.07	0.82	0.43	0.05	0.06	0.1	0.36
K_2O (%)	0.88	0.1	0.27	0.46	0.26	0.34	0.11	0.19	0.04	1.06
P_2O_5 (%)	3.73	0.1	0.02	0.12	0.62	0.97	0.04	0.08	1.35	0.53
Ba (ppm)	6304	13.79	22126	8.1	99	2125	1229	2719	625	4096
V (ppm)	573	258	211	468	1637	39.8	144	106	874	94
Cr	247	10	7	16	186	13.6	13.7	10	18	15
Co	404	2	118	222	433	73.6	25.2	49.5	68.4	57
Ni	305	28	351	341	432	125	69.4	23	662	530
Cu	375	50	1174	691	500	95.6	154.9	126.8	553	86
Zn	580	26	129	147	374	60	66.7	63.5	288	154
Pb	2357	112	14	18	267	41	6.5	53.5	115	9.93
Th	31	2	2	98	4	-	0.4	433	2.45	2.13
Rb	24	2	3	4	5	18	2.9	5	1.62	11
Sr	-	85	483	260	102	2664	243	255	588	984
Y	-	5	-	-	80	14.8	33	22	136	54.8
Nb	-	3	8	4	4	-	0.7	11.1	3.94	0.08
Zr	-	12	62	48	104	49.4	4	26.9	88	4.29

Table 4. Rare earth element contents (ppm) and ratios of the Chiatura manganese-oxide deposit.

	Y	La	Ce	Pr	Nd	Sm	Eu	Gd	Tb	Dy	Ho	Er	Tm	Yb	Lu	ΣREE	$(Ce/Ce^*)_n$	$(Eu/Eu^*)_n$	$(Y/Y^*)_n$	$(La/Yb)_n$	Y/Ho
DL	0.01	0.5	0.1	0.02	0.02	0.02	0.02	0.02	0.02	0.02	0.02	0.02	0.02	0.02	0.02						
CH-1	53.1	59.4	118.9	15.05	60.76	13.74	3.96	12.35	2.27	11.82	2.44	6.36	0.87	5.76	0.75	314	0.91	1.44	0.79	0.76	21.8
CH-2	35.5	44.3	63.6	9.72	37.66	8.08	2.80	8.79	1.25	6.58	1.32	3.66	0.52	3.05	0.46	192	0.71	1.54	0.96	1.07	26.9
CH-3	36.7	30.7	42.6	6.64	26.93	5.84	1.63	7.01	1.04	5.94	1.21	3.39	0.47	2.66	0.37	136	0.70	1.17	1.08	0.85	30.4
CH-4	71.7	67.0	32.3	14.37	59.39	13.37	3.29	13.84	2.13	13.04	2.56	7.09	0.96	5.48	0.75	236	0.24	1.12	0.99	0.90	28.0
CH-5	27.1	26.7	29.6	5.17	21.97	5.30	1.26	5.25	0.78	4.27	0.89	2.49	0.34	2.22	0.31	107	0.57	1.13	1.11	0.89	30.5
CH-6	92.4	78.0	84.9	12.21	47.80	9.58	2.69	11.60	1.82	10.45	2.43	6.84	0.78	5.18	0.75	275	0.63	1.18	1.46	1.11	38.0
CH-7	137.3	62.8	59.8	12.47	54.63	11.30	3.30	15.25	2.50	14.85	3.37	9.26	1.15	6.92	1.01	259	0.50	1.15	1.54	0.67	40.7
CH-8	28.8	23.1	24.8	4.06	17.32	3.60	0.43	4.25	0.63	3.74	0.79	2.39	0.35	1.94	0.29	88	0.59	0.53	1.25	0.87	36.5
CH-9	27.5	28.3	21.0	4.56	18.49	4.14	0.66	4.71	0.69	4.25	0.90	2.60	0.35	2.41	0.34	93	0.41	0.69	1.15	0.87	30.5
CH-10	48.4	104	96.0	16.99	60.23	11.48	3.53	12.05	1.78	9.33	1.85	5.05	0.70	4.11	0.57	328	0.52	1.40	0.95	1.87	26.2
CH-11	37.4	30.5	37.4	8.45	35.41	7.34	2.61	8.51	1.37	7.42	1.46	3.97	0.57	3.58	0.51	149	0.53	1.54	0.91	0.63	25.6
CH-12	47.9	41.2	45.4	7.50	29.71	6.34	1.68	7.30	1.12	6.14	1.30	3.98	0.48	2.88	0.45	155	0.59	1.15	1.36	1.06	36.9
CH-13	30.4	25.2	31.3	4.44	18.88	3.80	1.17	4.66	0.71	4.22	1.03	2.80	0.43	2.60	0.37	102	0.67	1.29	1.18	0.72	29.5
CH-14	42.2	63.9	61.8	11.97	44.74	9.70	3.07	9.68	1.50	8.23	1.65	4.74	0.61	3.50	0.47	226	0.52	1.48	0.92	1.35	25.6
CH-15	78.3	25.5	43.4	7.64	41.85	12.02	3.31	15.31	2.49	15.39	3.34	9.16	1.40	8.78	1.22	191	0.71	1.12	0.87	0.22	23.4
CH-16	98.2	88.4	167.0	27.93	106.43	28.40	7.58	26.34	4.94	26.32	5.17	15.09	2.23	13.59	2.02	521	0.78	1.30	0.67	0.48	19.0
CHY-01	40.8	33.3	22.1	5.23	21.81	4.53	1.03	5.58	0.78	4.87	1.05	2.74	0.42	2.42	0.38	106	0.38	0.94	1.40	1.01	38.8
CHY-03	121.3	111	55.7	21.19	87.35	17.88	3.03	20.26	2.85	17.31	3.80	10.00	1.32	8.17	1.19	361	0.26	0.74	1.19	1.00	31.9
CHY-04	33.6	28.2	27.1	6.11	24.89	5.20	1.51	5.29	0.89	4.99	1.04	2.85	0.37	2.32	0.30	111	0.45	1.34	1.20	0.90	32.3
CHY-05	26.9	36.3	67.0	8.31	32.51	7.21	2.00	6.08	1.02	4.90	1.04	3.06	0.38	2.50	0.32	173	0.89	1.42	0.98	1.07	25.8
CHY-06	34.9	43.6	51.3	9.09	35.27	7.23	2.30	7.04	1.17	6.75	1.31	3.45	0.45	2.96	0.39	172	0.59	1.52	0.94	1.09	26.7
CHY-02	19.0	19.5	26.3	4.39	15.99	3.74	0.96	3.58	0.57	3.07	0.63	1.93	0.26	1.75	0.22	83	0.65	1.24	1.09	0.82	30.2
Average	53.2	48.7	55.2	10.2	40.9	9.1	2.4	9.8	1.6	8.8	1.8	5.1	0.7	4.3	0.6	199	0.58	1.20	1.09	0.92	29.8